ALMA MATER STUDIORUM - UNIVERSITÀ DI BOLOGNA
CAMPUS DI CESENA
DIPARTIMENTO DI
INGEGNERIA DELL' ENERGIA ELETTRICA E DELL'
INFORMAZIONE "GUGLIELMO MARCONI"

CORSO DI LAUREA IN INGEGNERIA BIOMEDICA

EVALUATION OF THE MICROSTRUCTURAL PATTERN AND MECHANICAL BEHAVIOUR OF HUMAN METASTATIC VERTEBRAE

Elaborato in
Comportamento Meccanico dei Biomateriali e delle Strutture (c.i)

Relatore
Chiar.mo Prof. Luca Cristofolini

Presentata da
Silvia Casadei

Correlatore
Dr. Marco Palanca
Dr. Enrico Dall'Ara
Ing. Giulia Cavazzoni

Anno accademico 2021/2022

Abstract

La spina dorsale è uno dei principali siti di sviluppo di metastasi ossee. Queste alterano sia la composizione strutturale che il comportamento meccanico delle vertebre metastatiche, riducendone la resistenza meccanica ed aumentandone il rischio di rottura. Questo studio ha valutato la composizione microstrutturale ed il comportamento meccanico a rottura in specifiche regioni all'interno di vertebre metastatiche.

11 segmenti vertebrali da cadavere, costituiti da una vertebra sana ed una con metastasi (litica, mista o blastica), sono stati testati con carichi graduali di compressione e scansionati con microCT. Le deformazioni interne sono state misurate tramite un algoritmo globale di Digital Volume Correlation (DVC). I risultati dall'analisi microstrutturale hanno mostrato l' influenza sulla microstruttura delle diverse tipologie di metastasi in corrispondenza della lesione, mentre le caratteristiche microstrutturali nelle regioni intorno alla lesione sono risultate simili a quelle delle vertebre sane. L'analisi delle deformazioni ha inoltre permesso di valutare l' effetto delle diverse tipologie di metastasi nel compromettere la stabilità spinale. Le vertebre con metastasi litiche hanno raggiunto deformazioni maggiori in corrispondenza della lesione, regione meccanicamente più debole e con una microstruttura maggiormente compromessa a causa della metastasi. Le vertebre con metastasi blastiche hanno raggiunto deformazioni minori nella lesione, regione che ha mostrato una maggiore resistenza meccanica ai carichi, e deformazioni maggiori nelle zone più lontane. Le vertebre con metastasi miste hanno mostrato un comportamento meccanico non univoco, legato alla predominanza di una lesione sull'altra. Infatti, la posizione e la proporzione tra le due lesioni sembra influenzare il comportamento meccanico. I risultati di questo studio, una volta generalizzati, potrebbero portare alla spiegazione delle cause di instabilità meccanica nelle vertebre metastatiche.

Parole chiave: metastasi spinali; instabilità spinale; microCT; analisi regionale; analisi microstrutturale; composizione microstrutturale; Digital Volume Correlation, analisi deformazioni

Abstract

Spine is one of the most common sites for bone metastases. The presence of metastases may alter the microstructure pattern and the mechanical behaviour of the vertebrae. Metastases may reduce load-bearing capacity and increase the risk of fracture but the effect of the different types of metastases (i.e. lytic, blastic and mixed) is still unclear.

In this study, I aimed to evaluate the microstructural pattern and mechanical properties at failure in specific regions of interest within human metastatic vertebrae. Eleven human spine segments with different types of metastases (lytic, blastic and mixed), consisting of a healthy and metastatic vertebra, were prepared and scanned with microCT in step-wise compressive loadings. Regional analysis was performed to evaluate the changing in the microstructural pattern in different regions of the metastatic vertebrae. The internal strain field was computed using a global Digital Volume Correlation approach to evaluate the mechanical behaviour.

The microstructural results showed the different influence of the different types of metastases on the microstructural pattern in correspondence of the lesions. In addition, the microstructural features in regions surrounding the lesions were found similar to healthy vertebrae. The strain analysis showed how different types of metastases have a different influence in triggering the stability of the spine. Vertebrae with lytic metastases reached higher strain in correspondence of the lesion, region that is weaker and more compromised in the microstructure due to the lack of bone tissue and microstructural features. Vertebrae with blastic metastases reached lower strains in correspondence of the lesion and higher strains far from the lesion. In this case, the region correspondent to the blastic metastases presents a higher resistance to loads-bearing. Mechanical results on vertebrae with mixed metastases show an unregular trend, influenced by the predominance of one lesion to the other. Indeed, position and proportion between the two lesions can affect the mechanical behaviour of vertebrae with mixed metastases. The outcomes of this study, once generalized, could lead to an explanation of the mechanical instability of the spine, due to the presence of vertebrae with metastases.

Key words: spinal metastases; spinal instability; microCT; Regional analysis; microstructural analysis; microstructural pattern; Digital Volume Correlation, strain analysis

Contents

CHAPTER 1: INTRODUCTION

1.1 VERTEBRAL METASTASES

The spine is the first site for incidence of bone metastases. Metastases are divided into three types: lytic, blastic and mixed [1]. Using computed tomography it is possible to evaluate the different features of each type of metastases. Lytic metastasis presents bone reabsorption and is characterized by voids. In this case, the metastases are visible as black holes in the vertebral body in the radiological images (Fig 1.A). The characteristic of blastic metastasis, instead, is the growth and the thickening of new tissue which is easily seen in radiological images as a brighter portion in the vertebral body, due the higher bone density (Fig. 1.B). Mixed metastases present both types of lesions, lytic and blastic (Fig 1.C, 1.D). In radiological images, voids and brighter portions are both present: brighter portions represent blastic metastasis and darker portions represent lytic metastasis (Fig 1.C).

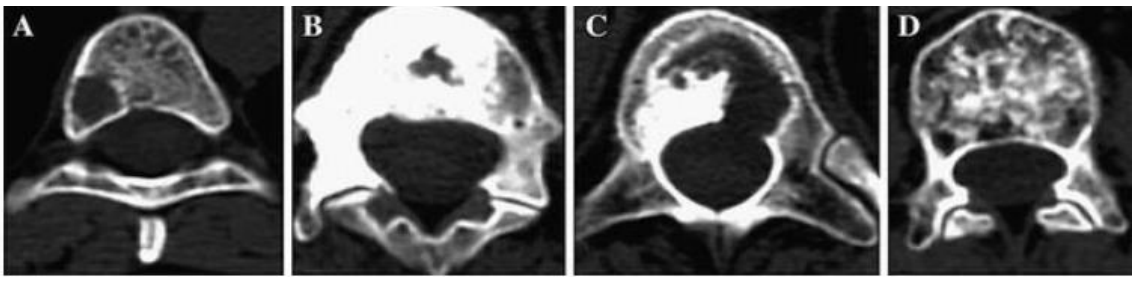

Figure 1*:* CT scan of human vertebrae with lytic metastasis (A), blastic metastasis (B), mixed localized metastasis (C) and diffuse mixed metastasis (D) [1].

Therefore, each kind of metastases is characterized by a different organization of the bone tissue that leads to different mechanical behaviour and by a change in the bone remodelling process. In fact, the presence of metastases deteriorates and decreases the optimization of the bone structure. The lack of optimization and the alteration of the bone remodelling process compromise the mechanical properties.

Bone metastases can cause severe problems in daily life of patients as pain, fractures, life threatening hypercalcemia and nerve compression symptoms [2]. All these aspects lead to a worsening of the quality of life in yet debilitated patients. Lytic metastases have a known and predictable mechanical behaviour: the bone reabsorption causes a decrease of bone density leading to a decrease of mechanical strength, as demonstrated in several

studies [3]. Instead, in case of blastic tissue, the situation is still unclear. The increase of bone formation may lead to a higher resistance to load bearing but the mechanical property of the new added tissue is unknown. General hypothesis about blastic tissue is that it may be not organized, may be constitute by poor quality material, and the bone structure may not be optimized. Moreover, the increased quantity of tissue may cause damage and increase risk of fracture in the regions close to the lesion.
Clinically, the presence and type of lesions may be diagnosed with imaging techniques such as Computed Tomography scan (CT), Magnetic Resonance Imaging (MRI), or Positron Emission Tomography scan (PET), and ultimately be confirmed by bone biopsy and histological analysis. However, imaging methods are not efficient in many cases to diagnose and distinguish metastasis, because are operator-dependent and in some cases, metastatic disease can be mistaken for shrinking/enlargement of trabeculae.

1.2 CLINICAL ASSESMENT

The treatment of spinal metastases involves a multidisciplinary approach with several options such as radiations, surgery, medical oncology, and a combination of these techniques with the aim of pain relief, local tumour control, spinal stability, and improvement in daily life. However, the treatment of the metastasis is only palliative, with the goal of improving the patient life quality [4]. In the past decade, there has been an evolution concerning treatment thanks to the development of the NOMS, framework for metastatic spine disease that includes four assessments (neurologic, oncologic, mechanical, systemic) to determinate the best treatment [4]. To help clinicians in understanding when patients need to refer to orthopaedic consultancy, the Spine Instability Neoplastic Score (SINS) was developed in 2010 by the Spine Oncology Study Group [5] to assess the degree of spinal stability caused by the metastatic disease. The score consists in the sum of 6 parameters: 5 radiographical parameter (spine location, bone lesion quality, spinal alignment, vertebral body collapse, posterolateral involvement of spinal elements) and 1 clinical parameter (mechanical Pain) (Table 1). The clinical component considers whether patients have mechanical pain associated with the neoplasm.

Table 1: Parameters and value of the score SINS [5]

Characteristic	Score
Location	
Junctional (occiput–C2, C7–T2, T11–L1, L5–S1)	3
Mobile spine (C3–C6, L2–L4)	2
Semi rigid (T3–T10)	1
Rigid (S2–S5)	0
Pain[a]	
Yes	3
Occasional pain but not mechanical	1
Pain-free lesion	0
Bone lesion	
Lytic	2
Mixed (lytic/blastic)	1
Blastic	0
Radiographic spinal alignment	
Subluxation/translation present	4
De novo deformity (kyphosis/scoliosis)	2
Normal alignment	0
Vertebral body collapse	
>50% collapse	3
<50% collapse	2
No collapse with >50% body involved	1
None of the above	0
Posterolateral involvement of spinal elements[b]	
Bilateral	3
Unilateral	1
None of the above	0

[a]Pain improvement with recumbency and/or pain with movement/loading of spine.
[b]Facet, pedicle, or costovertebral joint fracture or replacement with tumor.

Score range is 0-18 and is divided into three categories: 0-6: stable7-12: potentially unstable 13-18: unstable (Table 2).

Table 2*:* SINS scores organized as a total score, three-clinical categories, and binary scale with their corresponding levels of stability [5]

Total Score (0-18 SINS)	1	2	3	4	5	6	7	8	9	10	11	12	13	14	15	16	17	18
Three Clinical Categories (3-point)			Stability					Potentially Unstable							Unstable			
Binary Scale (2-point)			Stability					Current or potential instability; Surgical consultation recommended										

The SINS should help specialists in optimizing treatments for patients and choosing whether the patient can benefit and support a surgical intervention or benefit from other options, like radiotherapy. Oncologists are not bound to follow the SINS but is recommended to consider a surgical consultation in case of score equal or higher than 7 [6]. However, SINS has a great grade of uncertainty, in fact most cases fall in the potential unstable category, where there are no clear guidelines to follow. The problem of the SINS is the lack of specificity and the fact that it does not consider important metastatic features such as size and position of the metastases, but only the types of them (blastic, lytic). A study by Palanca et al. [3] was conducted to validate the correlation between type, size and position and mechanical assessment in metastatic vertebrae and control vertebrae. It has been demonstrated, in fact, that type, size and position affect the deformation of metastatic vertebrae under different loading conditions. The results also showed that the SINS did not correlate with the position and the size of the metastatic vertebrae. This result is coherent with the work of Costa et al. [7]. This study demonstrated that there was no relation between SINS and behaviour of human lytic vertebrae. Both studies highlight that the major clinical tool used to define spine instability has no mechanical evidence.

1.3 MECHANICAL INVESTIGATION OF THE SPINE

Regarding the mechanical assessment, according to author's knowledge, spine is probably one of the most complex structures of the skeleton to study [8]. The major and common approach to evaluate mechanical properties in vitro is the "invers approach".
The spine is composed by sequences of hard (vertebrae) and soft (intervertebral discs) tissues, stabilized by ligaments [9]. Thus, different types of specimens can be used (Fig. 2). Specimen can be spine segments, and in this case, ligaments, disc and articulating surface may not be removed to better replicate physiological condition. To evaluate structural properties of the single vertebral bone, pedicles can be removed (vertebral body) or not removed (whole vertebrae). In the first case soft tissues are removed, and loads are applied directly on the surface of the vertebral body or on the endplates, usually embedded with PMMA or other materials to hold fixed specimen during the test [9].

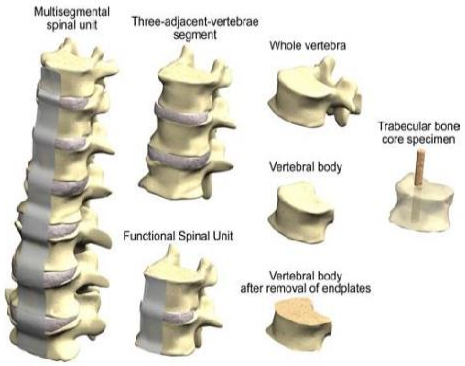

Figure 2: spine samples used in vitro test [9]

In vitro experiments must be repeatable, reproducible, and consistent. For this reason, animal specimens are frequently used to design the experiment instead of human ones, which are difficult and complex to obtain due to ethical and bureaucratic restriction; in addition to the fact that humans present a great variability in terms of gender, age, pathologies, ethnicity, and other factors while animal models are largely more homogeneous [9]. Nevertheless, there are several anatomic differences within quadrupeds and humans, considering dimensions (human vertebral body is shorter and wider than most quadrupeds) and microstructure (quadrupeds are denser with higher bone mass than humans). Lastly, animal models have different physiological condition because their spine is optimized for bending, whereas humans are mostly subjected to axial compression [9].

In vitro local strain analysis can be divided into pointwise or full field. In the first case, strain gauges are the most used technique to measure deformation on the specimen. Strain gauges are cheap and simple to use but they have several disadvantages. Firstly, they are operator dependent due to the fixation on the specimen. In addition, strain gauges cannot be used on soft tissues because of their intrinsic strength. Lastly, the deformations are quantified only in the small areas covered by the strain gauges, this fact leads to a loss of information in the nearby and far areas. Some studies have focused on the mechanical characterization of metastatic vertebrae. It has been widely reported [4], [7] that vertebrae with lytic metastases present lower stiffness and strength compared to the healthy vertebrae with higher strains in correspondence of the lesion, which leads to a higher risk of fracture. Blastic lesions should have higher strength than lytic lesions due to the denser portion [3], [10] but their mechanical behaviour is still unclear.

To evaluate deformation in all the specimen and create a continue map, other digital techniques are used, like Digital Image Correlation (DIC) and Digital Volume Correlation (DVC). In 2020, Palanca et al. [11] carried out a study with the aim to evaluate the effect of artificially induced lesions (Fig. 3) on the strain field inside porcine vertebral bodies tested in compression. The creation of artificial lesion was aimed to simulate the lack of bone density caused by lytic metastases. The artificial lesion reduced strength and mechanical properties, causing, in some cases, failure.

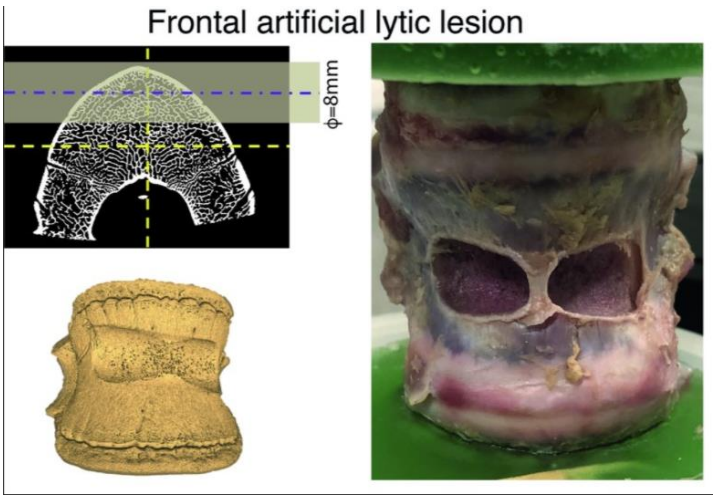

Figure 3: porcine vertebrae with artificial lesion to simulate lytic lesion [11]

Just few studies used the DVC approach to study the biomechanics of the vertebrae with actual metastases. The first of them [12] involved vertebrae with lytic metastases. Ten specimens of rat with induced tumour with the progressive formation of lytic lesions were scanned with micro-CT in compressive loading condition and the internal strains were

compared with the ones of control (healthy) vertebrae. The results confirmed showed that metastatic vertebrae reached higher compressive strains (over two times) than control ones and the regions with higher strain concentrations were the regions compromised by lytic metastasis (scanned with CT), as showed for the healthy vertebra in Figure 4 and the vertebra with lytic lesion in Figure 5. This demonstrates the effect of lytic metastases on the mechanical assessment: the lack of bone tissue due to the metastasis and the consequently loss of bone density lead to a reduction in the load bearing and an increase of strain in correspondence of the lesion.

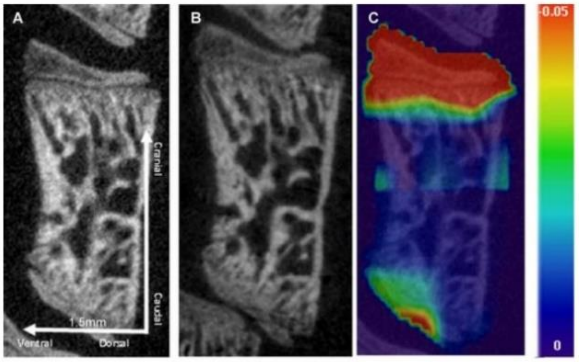

Figure 4: central sagittal section of healthy vertebra in the unloaded configuration (A), central sagittal section of healthy vertebra in the loaded configuration (B). central sagittal section of healthy vertebra in the unloaded configuration overlaid with axial strain measured by image registration (C) [12]

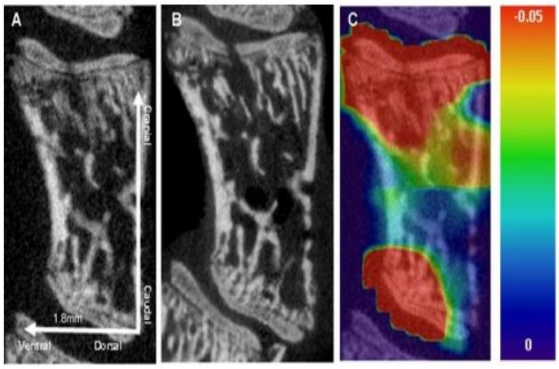

Figure 5: central sagittal section of lytic vertebra in the unloaded configuration (A), central sagittal section of lytic vertebra in the loaded configuration (B). central sagittal section of lytic vertebra in the unloaded configuration overlaid with axial strain measured by image registration (C) [12]

The only work that aimed to evaluate the mechanical behaviour of human metastatic vertebrae using micro-CT and DVC was proposed by Cavazzoni in her master thesis [13].

The vertebrae presented mixed, blastic and lytic metastases. The internal strain field obtained by DVC in elastic region was evaluated into metastatic and adjacent control vertebrae (Fig. 6). Generally, vertebrae with lytic metastases showed larger strain than control one, as expected. In case of blastic and mixed metastases, a regular trend was not observed. Some specimens with blastic metastasis showed lower deformations than healthy tissue, while other showed larger deformations. However, as blastic metastases are characterized by denser tissue, portions with denser trabecular patterns were expected to be stiffer to loads bearing.

This unexpected behaviour can be explained by investigating the microstructure of the metastatic tissue, which seems to play an important role in load bearing. Nowadays, the role of microstructure on the mechanical behaviour is still unclear. In fact, a correlation between the strain field and microstructural parameters is missing but necessary to better evaluate and study the mechanical properties. In addition, this work measured the local strains in regions of interest without considering that in some cases blastic and lytic metastases could be present in the same portions. Consequently, the opposite behaviours of metastases were observed. A solution to this problem could be isolating the lesion from the healthy part of the vertebrae and evaluating the microstructural and mechanical features only in the area involved with the lesion, to focus the analysis only in the metastatic area. This last approach has never been investigated with DVC. Another lacking aspect regarding the use of DVC applied to metastatic human vertebrae is the evaluation of internal strain field in the tissue nearby the metastasis to study if there is an influence of the lesion in the adjacent regions.

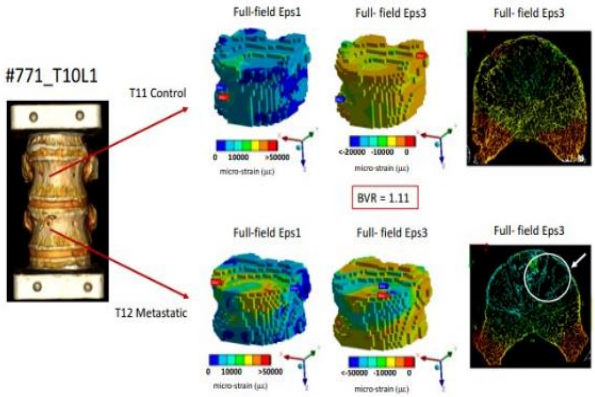

Figure 6: maps of strain in the internal of control and metastatic vertebrae. In the right bottom corner, in correspondence of the lytic lesion the strains are higher in comparison with the control vertebrae [13]

1.4 DIGITAL VOLUME CORRELATION

Digital volume correlation (DVC) is a novel technique for the measurement of the internal three-dimensional deformation across the entire volume of various biological tissues, such as bone [14]. DVC was originally developed by Bay et al. [14] to investigate the volumetric strain distribution throughout the bone trabecular structure.

The principle of the DVC is based on a combination of imaging and mechanical test. Images of the specimens are acquired in unloaded and loaded condition with 3D imaging techniques (microCT, MRI, qCT). The DVC takes advantage of the natural internal pattern of specimens, obtained with the 3D scans (Fig. 7). Thanks to this approach, can be evaluated internal displacement and strain.

Local and global DVC approaches can be applied. A local approach involves the study of small subregions and independently correlates. In this case, for each subregions the displacement field is evaluated in the central point [15]. A global approach involves the entire image of the whole specimen. Displacements are computed dividing the entire volume in a 3D grid and displacement are evaluated in the nodes [16].

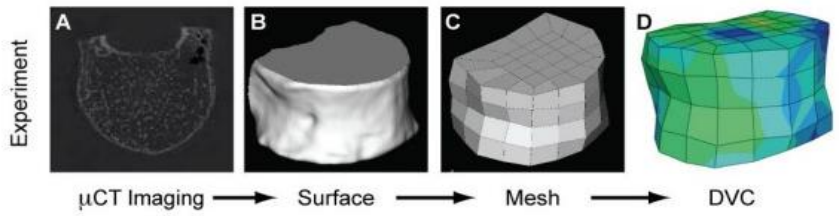

Figure 7: computational process to obtain DVC map of strain [17]

DVC is affected by several parameters such as: investigated microstructure, subject size, objective function, image voxel size [17]. Accuracy and precision depend on the approaches and the optimization of the DVC parameters. To evaluate the precision and accuracy of DVC approaches, test in zero strain condition have been carried out. A study conducted by Palanca et al. [15] compared three different DVC approaches (Fig. 8). Results showed that ShIRT-FE, later known as BoneDVC, based on global approach on elastic registration and a finite element solver was the best in term of accuracy and precision. In addition, it has been noted that accuracy and precision increase with an increase of the sub-volume size and the nodal spacing, with a consequential deterioration of the spatial resolution. Palanca et al. [15] used cortical and trabecular bone specimen

highlighting the differences between the types of specimens. It has been observed that the accuracy of strain measurements is influenced by the nature of the investigating tissue.

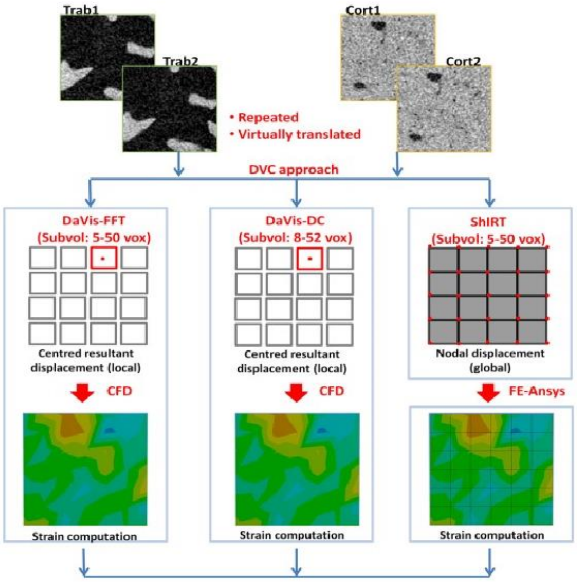

Figure 8: description of the three DVC approach [15]

This result is coherent with the work of Liu and Morgan [16], in which multiple types of trabecular bone (bovine distal femur, bovine proximal tibia, rabbit distal femur, rabbit proximal tibia, rabbit vertebra, and human vertebra) were tested. Accuracy and precision were defined as the mean absolute error (MAER) and the standard deviation of the error (SDER) [16]. They were quantified as the mean and the standard deviation of the average of the absolute values of the six strain components for each sub-volume:

$$\text{MAER}=\frac{1}{N}\sum_{k=1}^{N}\frac{1}{6}\sum_{C=1}^{6}\left|\varepsilon_{C,k}\right|$$

$$\text{SDER}=\sqrt{\frac{1}{N}\sum_{k=1}^{N}(\frac{1}{6}\sum_{C=1}^{6}\left|\varepsilon_{C,k}\right|-\text{MAER})\text{^}2}$$

Equation 1: calculus of accuracy and precision

is the strain; "c" represents the strain component; "k" represents the point of measurement; "N" is the total number of measuring points.

The use of DVC to investigate the strain distribution in vertebrae has been firstly introduced by Hardisty and Whyne [18] to spatially resolve strain in rat vertebrae using microcomputed tomography (CT) images. In the literature, several studies have been

carried out to evaluate the internal strain field of healthy vertebrae, using micro-CT and MRI as imaging techniques. A study involving three porcine thoracic vertebrae [19] loaded in a stepwise fashion at increasing steps of compression (5%, 10%, 15%) showed the important advantage of DVC of quantifying internal microdamage in the bone microstructures. The results clearly showed how local strain built up from the elastic regime and highlighted those internal weaker regions that could result in microdamage initiation and progression up to vertebral failure. The internal strain distribution obtained by DVC showed that the most strained region corresponded to the damaged area (compression 15%) and showed that an increase of loading compression led to an increase of strain which gradually propagate in the vertebral body (Fig. 9).

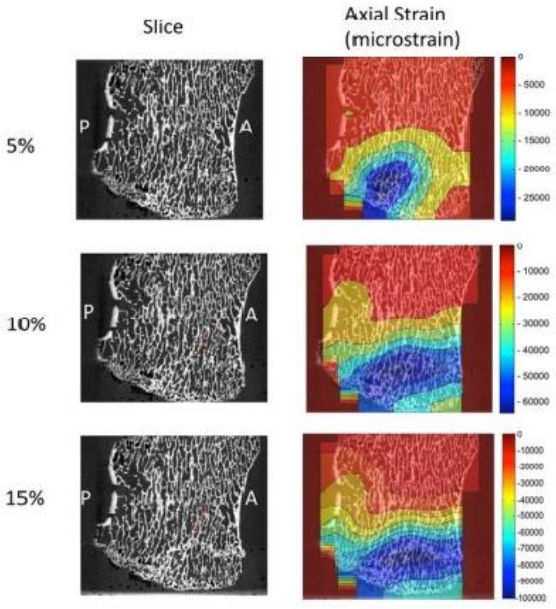

Figure 9*:* map of strain distribution in porcine vertebrae in different case of loading compression (5%,10%,15%). The image shows the progression and increase of strain with the increase of loads [19]

Recently lots of work have been focused on the use of DVC to measure internal strains of vertebrae in zero-strain and loading conditions. A study by Palanca et al. [20], aimed to measure the uncertainty of different approaches of DVC (global and local) in porcine augmented and natural vertebrae in a zero-strain condition. An important result was the independence of errors from the specimen and scan direction, as the systematic and random errors did not show any correlation with the scan direction and/or specimen directionality. The relation between random errors and sub-volume size is coherent with previous works. For both approaches and both natural and augmented vertebrae with an increase of sub-volume size there is an evident reduction of errors (Fig. 10).

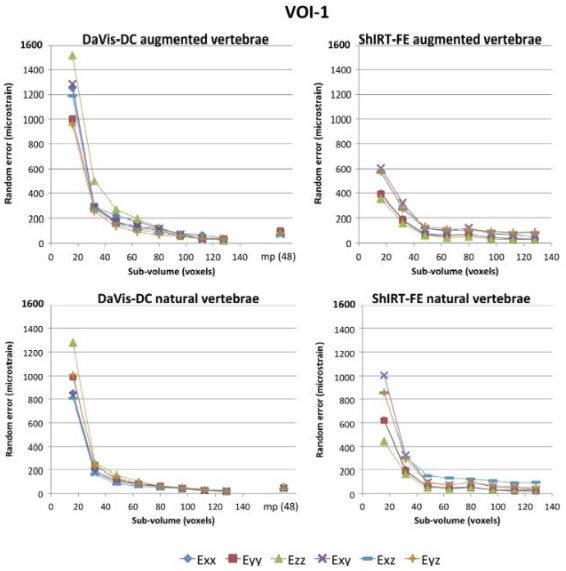

Figure 10: relation of random errors and sub-volume size in porcine natural and artificial vertebrae and the use of two DVC approaches (DaVis-DC and ShIRT-FE). The image shows that the increase of sub-volume size leads to a reduce of random errors for both approaches and both types of vertebrae [20].

Regarding metastases, DVC could be used to:

- detect the progression of failure in metastatic bones such as the vertebra;
- measure, for the first time, the deformations that occur throughout the vertebra during activities of daily living and during trauma;
- linked to the spine metastases, to compare the internal strain field of healthy and metastatic vertebrae;
- study the micro-damage evolution of metastatic vertebrae due to the disease.

Such measurements are relevant for studies of whole metastatic bone failure mechanisms and bone adaptation.

1.5 MICROSTRUCTURAL INVESTIGATION

The microstructural investigation of internal bone tissue relies on the evaluation of the trabecular pattern. One of the most used technologies to visualize trabecular bone microstructure is micro-CT, with the advantage to obtain 3D measurements without

destroying the specimens [21]. There are lots of parameter that can be evaluated to study the trabecular pattern. The most frequent in the literature are: Bone Volume (BV), Bone Volume Fraction (BV/TV), Trabecular Thickness (Tb. Th.), Trabecular Number (Tb. N.), Trabecular Spacing (Tb. Sp.) and Bone Mineral Density (BMD).

The Parfit model was firstly used to assess bone quality measuring the architecture of trabecular bone. The Parfitt plate model calculates trabecular thickness, spacing and number using formulae derived based on bone volume and surface area:

$$Tb.N = \frac{\frac{BV}{TV}}{Tb.Th}$$

Equation 2: calculus of trabecular number

This model is limited to the structural assumption that all trabeculae are plates, which is a limitation particularly in the consideration of low-density trabecular bone or bone compromised by pathology such as lytic metastases. A structural- independent methods was proposed by Hilderbrand and Rüegsegger [22], defying trabecular thickness at every point as the diameter of the biggest sphere that could perfectly fit inside the trabeculae.

Microstructural investigation is a powerful tool that can be linked and correlated with mechanical properties. Failure strength and loads bearing depend on the quantity and structure of the considered materials. It is generally accepted that the mechanical strength of trabecular bone depends on both bone mass and bone quality [23], [24]. In addition, regarding the correlation between mechanical properties and microstructural parameters of healthy vertebrae, some previous experiments have established that failure strength of vertebral bodies is predominantly affected by bone volume fraction and bone density [25]. Other studies [26] [27] have reported significantly high correlations between the microstructural indices of trabecular bone in two dimensions, but there is a huge lack regarding correlation between 3D data because they are not easy to obtain. In particular, the mechanical response is highly affected by the density of tissue. In case of vertebral lesion, several studies have reported the changing in bone density due to the lesion. In fact, metastasis can be described in term of bone density. Blastic metastases are characterized by growth of new bone tissue which highly increase the bone density, whereas lytic metastases present bone reabsorption that leads a loss in bone density [2].

In general, metastatic lesions change the structural integrity of bones and the effect of metastasis on the trabecular pattern has already been reported in literature [28], [29].

Wise-Milestone et al. found significant difference in microstructural parameters between the control and metastatic rat vertebrae. The lytic nature of metastatic involvement has been shown to impact microarchitecture of trabecular bone, reducing the number and thickness of trabeculae, and reducing bone volume/total volume. Regarding blastic metastases in prostate cancer of human lumbar vertebrae [30], 3D analysis showed an increase in bone volume and in the number of trabeculae, without significative changes in trabeculae thickness in comparison with healthy vertebrae.

In the literature, the analysis of human trabecular microarchitecture on specific region of interest (ROI) was performed by Nagele at al [31] and Perilli et al. [32]. Nagele et al. [31] found variability in BV/TV Tb. Th, Tb. Sp, Tb. N due to the different anatomical site (Table 3).

Table 3: list of microstructural parameters in different anatomical sites [31]

	BV/TV [%]	Tb.Th [um]	Tb.Sp [um]	Tb.N [1/cm]
L2	10.2 ± 4.07	140 ± 14	986 ± 177	9.87 ± 1.65
Femoral Neck	20.6 ± 12.8	207 ± 57	951 ± 417	10.9 ± 3.29
Femoral trochanter	20.6 ± 12.8	143 ± 23	850 ± 263	11.8 ± 2.98
Distal radius	12.0 ± 7.10	148 ± 26	792 ± 113	12.0 ± 7.10

Perilli et al. [32] focused the microstructural analysis on lumbar healthy spine segment obtained by human cadaveric specimens, using micro-CT scan at 17 μm/voxel size. The microstructural parameters were computed in the whole vertebrae and in specific regions obtained by dividing the vertebra in subregions: posterior, middle, anterior, inferior, central, and superior (Fig. 11). Results show heterogeneity in the tissue distribution.

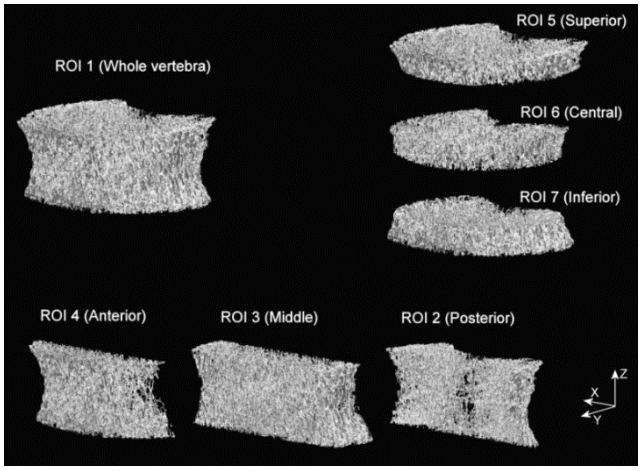

Figure 11: specific region of interest (ROI)s of human lumbar vertebrae, in which microstructural parameters were calculated [32]

Nevertheless, a correlation between the mechanical assessment and the microstructure in metastatic human vertebrae is missing but necessary to quantify the effect of microstructural metastatic feature on the mechanical properties. This aspect may lead to an evolution in clinal field. Evaluating the mechanical assessment using microstructural parameter may let to a previous and better knowledge of those regions that could cause the fracture.

1.6 AIM

The aim of this study is to evaluate the effect of the microstructural features on the mechanical properties of human metastatic vertebrae by measuring the correlation between the 3D strain field inside the vertebrae and the microstructural parameters. The hypothesis is that the local microstructure can affect the mechanical behaviour of metastatic vertebrae. In particular, the microstructural analysis on the micro-CT images was performed in specific regions: near the lesions, far from the lesions, and within the lesions. The internal strain field in metastatic vertebrae, tested in pure compression until failure, was measured using a global algorithm of DVC, called BoneDVC, in the same specific regions.

CHAPTER 2: MATERIALS AND METHODS

2.1 SPECIMEN PREPARATION

The procedures were all approved by the ethics committees of Bologna [33] and Sheffield [34], in accordance with the Declaration of Helsinki. The specimens were obtained by cadaveric human spines affected by bone metastases through an ethically approved international donation program (Anatomy Gift Registry, USA). Donors were adults with different sex, age, weight, and height and different type of metastases, diagnosed by orthopaedics. Orthopaedics, also, evaluated SINS for every metastatic lesion without considering the mechanical pain.

The specimens consisted in spine segments of four vertebrae: a healthy vertebra (later referred to as control) and metastatic vertebra in the middle, delimited by two vertebrae at the extremities. Due to the small space available to perform the in situ mechanical tests the posterior elements of each specimen were removed by cutting the specimens in the middle of the vertebral arch in the cranio-caudal direction.

In this study, eleven specimens have been analyzed: five with lytic metastases, two with blastic metastases and four with mixed metastases.

2.2 IN SITU MECHANICAL TESTS

Acquisition and mechanical test were previously performed at the Medical School (University of Sheffield, UK) by Eng. Giulia Cavazzoni and, -Dr Marco Palanca, co-supervisors of this project.

Each spine segment was scanned using micro-CT (VivaCT80, Scanco Medical, Bruttisellen, Switzerland) with a set of parameters used in a previous study on porcine vertebrae [11]: current 114 μA, voltage 70 kVp, integration time 300 ms, power 8 W, isotropic voxel size 39 μm. To reduce the beam hardening artefact a polynomial correction based on scans of a wedge phantom with 1200mg/ cm^3 of hydroxyapatite (HA) was used during the reconstruction step.

Each specimen was tested in step-wise compression loading inside a custom-built jig, consisting of a Plexiglas tube with low X-Rays attenuation (Fig. 12). The loads were manually applied outside the CT chamber by means of a torque wrench.

At first a preload of 50N was applied to ensure the stability of the specimen inside the loading device and the specimen was scanned (unloaded condition). Then the specimen was loaded up to failure and scanned again (loaded condition).

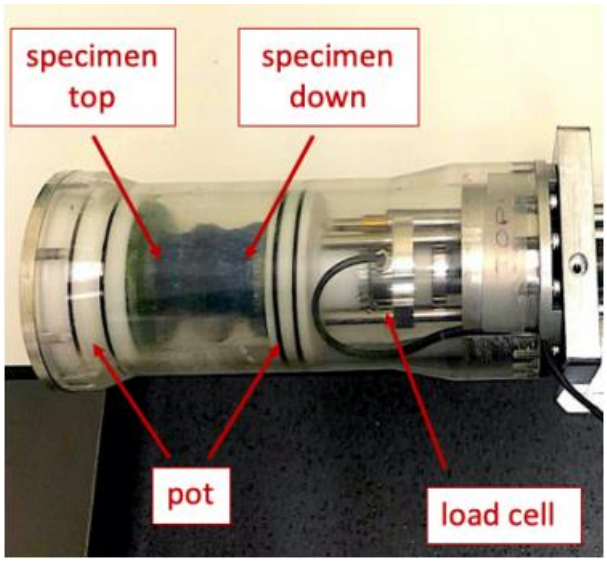

Figure 12: specimen inside the custom-built jig [13].

2.3 CTANALIZER

The microstructural 3D analyses were performed using CTAnalyzer software (CTAn). CTAn allow us to evaluate several microstructural parameters. Regarding our study, the chosen parameters to compare among lytic, mixed and blastic lesions were: the bone volume fraction BV/TV (%), the Trabecular Thickness Tb. Th (μm), the Trabecular Separation Tb. Sp (μm), and Trabecular Number Tb. N (1/mm).

2.4 BONEDVC

BoneDVC is a global DVC approach. It combines two algorithms: an elastic registration software ShIRT (Sheffield Image Registration Tollkit) and a Finite Element software package (Ansys v.14.0, ANSYS, Inc., Canonsburg, PA). The aim of BoneDVC is to measure the displacement and strains fields inside a structure. Two 3D images (micro-CT images), of the specimen in unloaded (fixed image) and loaded (moved image) conditions, are uploaded. An imposed and homogenous 3D grid is applied to the 3D images. The match between images is obtained by minimizing the differences in terms of grey scales between fixed and moved image through a cost function. Thus, the

displacement is estimated in each node of the 3D grid. Finally, the strain field is computed deriving the displacement in Ansys (Fig. 13).

BoneDVC permits to evaluate the displacement and strain field in specific regions, through the addition of masks that specify where the registration should take place. The 3D homogeneous grid imposed on the two images is composed by cubes of 50 voxels (2 mm) side. If the nodes of grid fall inside the mask, the algorithm include the associated cubes in the registration of the strain field, otherwise if the nodes fall outside the mask, the cubes are excluded from the registration.

The global approach of DVC was proved to be the best in terms of accuracy and precision in the measurement of internal strain in the vertebral body [17], [22].

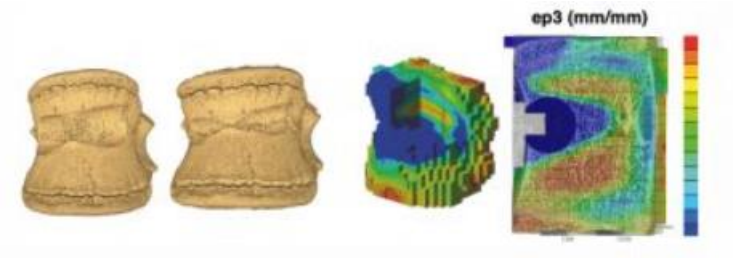

Figure 13*:* strain field in artificial lesioned and in healthy vertebrae computed with Ansys [17].

2.5 REGIONS OF INTEREST

2.5.1 MASKS OF THE LESION

A manual segmentation of each microCT scan was performed to select the whole volume of the vertebra and the whole volume of the lytic and blastic lesions within the vertebra. Firstly, for each specimen, lesion masks have been created applying threshold values to isolate the lesion, both for lytic and blastic metastasis. Using ImageJ's threshold tool it was possible to identify the different grey levels of each structure: background 0, vertebral body 1, lytic metastasis 2 and blastic metastasis 3 (Fig. 14).

In case of mixed metastases, two different masks were created: one for the lytic and one for the blastic lesion (Fig. 15).

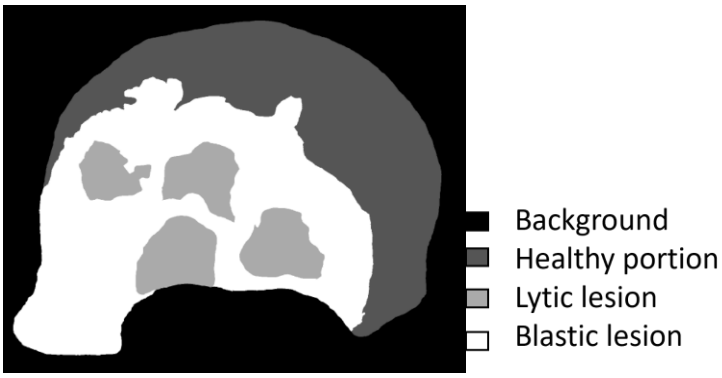

Figure 14*:* image of 776_L4 specimen. The white portion represents blastic lesion (value 3), the lighter grey represents the lytic lesion (value 2), the darker grey represents the vertebral body (value 1), the black represents the background (value 0)

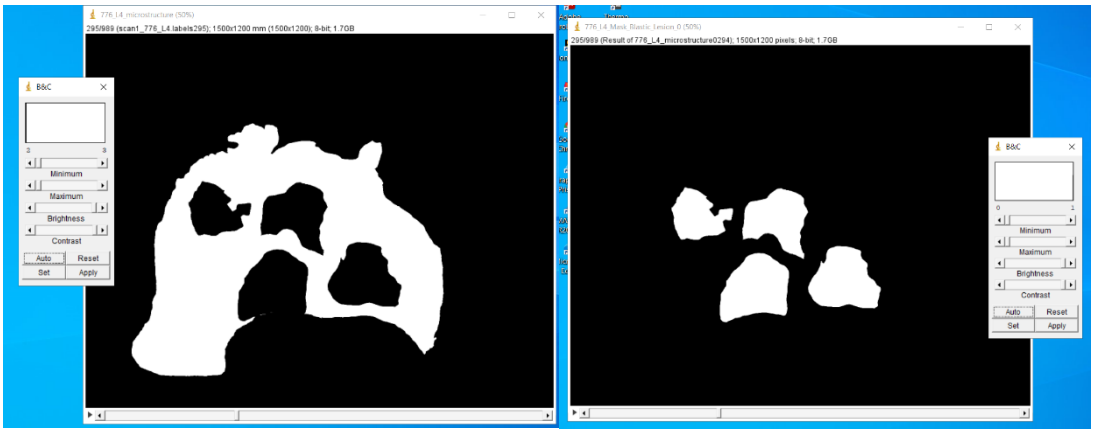

Figure 15*:* mask of mixed lesion of 776_L4 specimen. Left blastic lesion, right lytic lesion

2.5.2 MASKS SURROUNDING THE LESION

Then the masks in the area surrounding the lesion were created. The enlargements of the lesion mask were created using a binary function of ImageJ, named *Dilate*. The function *Dilate* adds a specific and chosen number of pixels in the transverse plane to the boundary of objects.

In this study, starting from the lesion mask, the enlargements were created by dilating of 100 pixels (100*0,039 mm=3,9 mm) at each step. The masks of enlargements were created until an enlargement that covered the entire cross section of the vertebral body was created (Fig. 16). The number of enlargement masks to create depends on the size of the lesion: the more extended the lesion is, the less the number of enlargements. For example, the maximum number of enlargements was 7 (the lytic lesion was dilated of 700

pixel) in the specimens 771_T12 and 781_T12 and the minimum was 2 (the blastic lesion was dilated of 200 voxels) in the specimen 781_T7.

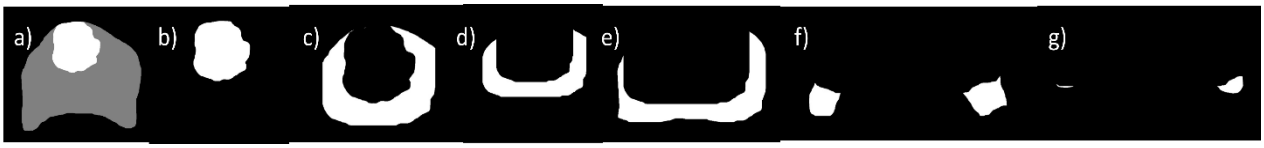

Figure 16*:* (a) mask of the whole vertebra in grey and of the lytic metastasis in white. (b) lytic mask. Enlargement of the lytic mask of 100 (c) 200 (d) 300 (e) 400 (f) 500 (g) pixels.

2.5.3 MASKS INSIDE THE LESION

In case of blastic lesion, the microstructural analysis can be performed also inside the lesion, where the bone is denser. The shrinkages were created using a binary function of ImageJ, named *Erode*. The function *Erode* removes a specific and chosen number of pixels in the transverse plane to the boundary of objects. In this study, the shrinkages were created by erosion of 100 pixels at each step. It was created one shrinking. As for the enlargements mask, the number of shrinking masks is not unique but depends on the size of the lesion: the more extended the lesion, the higher the number of shrinkages. Due to the small extension of the blastic lesions in the specimens, the shrinking has been made only once in five specimens: 777_L2 (Fig. 17), 771_T12, 776_L4, 781_T12 and 781_T7.

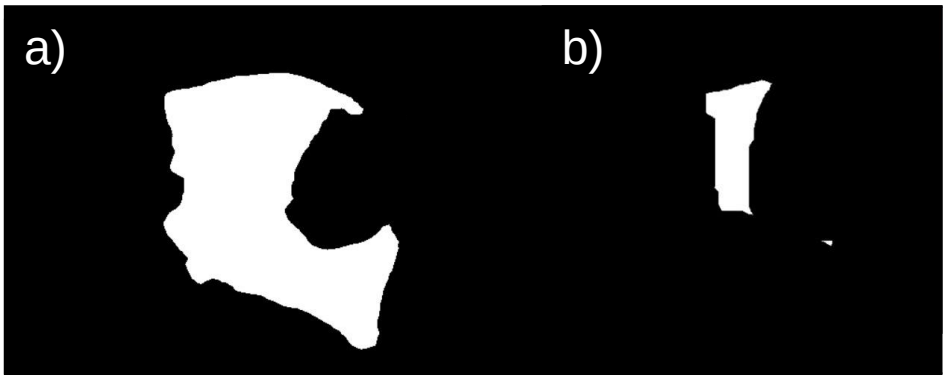

Figure 17*:* blastic lesion (a) and mask of the erosion of 100 voxels of blastic lesion (b) in 777_L2

2.6 METRICS

The evaluation of both microstructural and mechanical properties of metastatic vertebrae involved a local analysis and was carried out in specific regions of interest (ROIs):

- the region including the lytic (Fig. 18 b) or blastic lesion (Fig. 19 b)
- the region surrounding the lesions (enlargement) (Fig 18 c-g; Fig 19 d-g)
- the region within the blastic lesions (shrinkage) (Fig. 19 c)

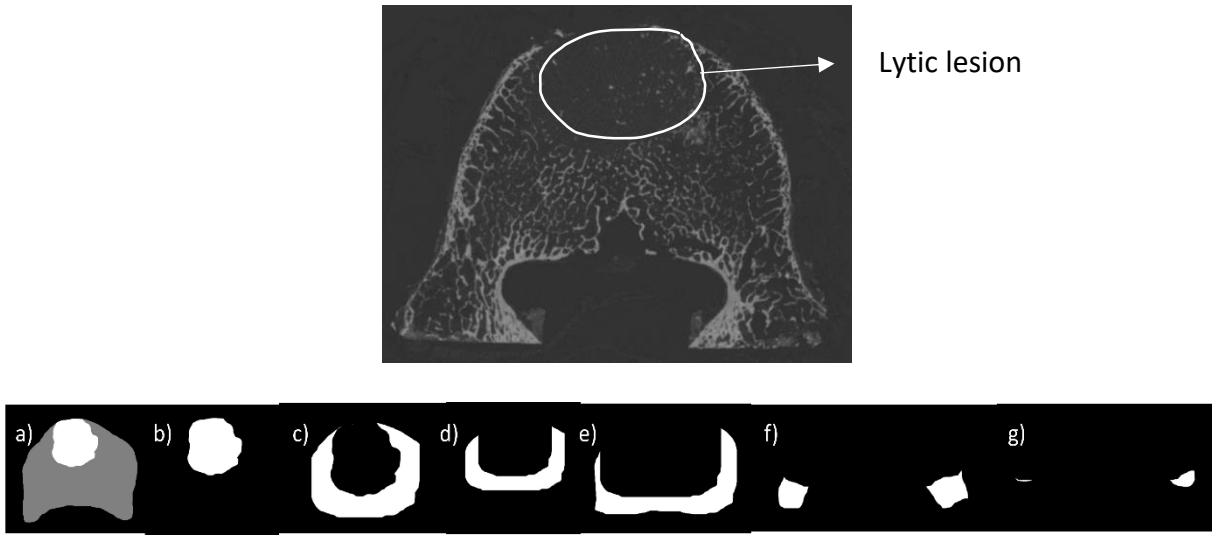

Figure 18*:* (a) mask of the whole vertebra in grey and of the lytic metastasis in white. (b) lytic mask. Enlargement of the lytic mask of 100 (c) 200 (d) 300 (e) 400 (f) 500 (g) pixels.

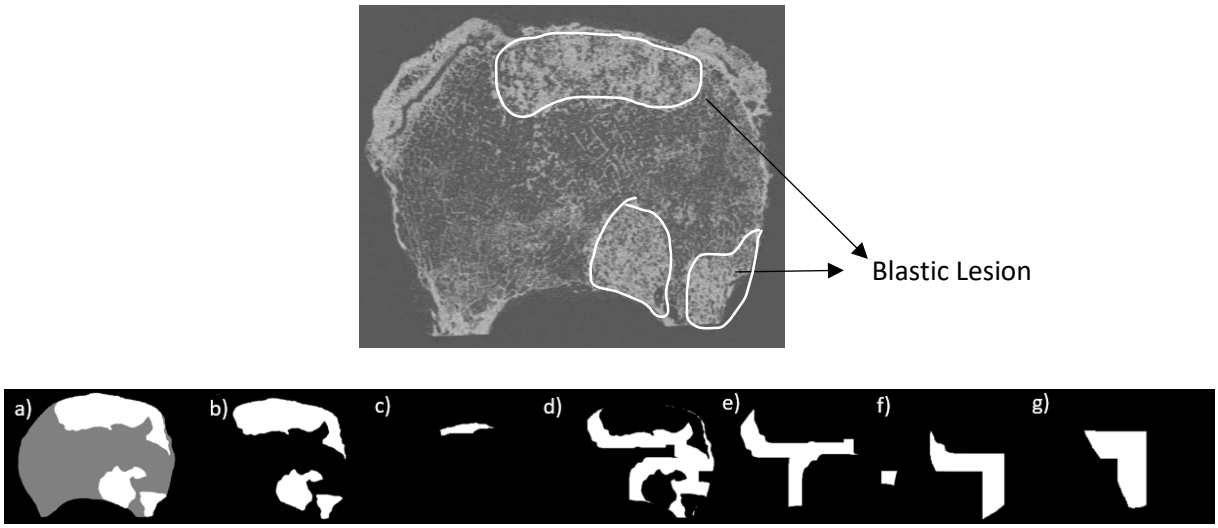

Figure 19*:* (a) mask of the whole vertebra in grey and of the lytic metastasis in white. (b) blastic mask. Shrinkage of the blastic mask (c).Enlargement of the blatic mask of 100 (d) 200 (e) 300 (f) 400 (g) pixels.

As regarding the microstructural analysis, the evaluation of BV/TV, Tb. Th., Tb.Sp. and Tb.N. was performed using CTAnalizer for eleven specimens. Normal distribution of the microstructural parameters was tested with the one sample Kolmogorov-Smirnov test (the data did not meet normal distribution). Mean values and standard deviation of microstructural parameters are reported for vertebrae with lytic, blastic and mixed on bar charts. Statistical analysis was performed to evaluate if there were statistically significant differences in the microstructural parameters among nearby and far areas from the lesion. Mann-Whitney test was used.

As regarding the mechanical analysis, internal strain field in the region of interest was computed with BoneDVC. Mean values of the minimum principal strains ($\varepsilon 3$) in each region of interest for each metastatic group were reported on bar charts. Statistical analysis was performed to evaluate if there were statistically significant differences in the minimum principal strains among nearby and far areas from the lesion. Mann-Whitney test was used.

All the statistical analyses were performed using Prism (Prism 9, GraphPad Software, USA) with the level of significance set to 0.05.

CHAPTER 3: RESULTS

3.1 MICROSTRUCTURAL ANALYSIS

The microstructural analysis was performed locally in specific region of interest for every specimen, calculating BV/TV, Tb. Th., Tb. Sp., Tb. N.
According to the orthopedics diagnosis, four out of eleven spinal metastases were classified as lytic, one as blastic and six as mixed. However, using the images scanned with micro-CT, it was possible to better identify and distinguish the lesions from the healthy tissue. Specimen 772_T11 and specimen 781_T7 were re-classified as affected by mixed metastases, whereas 772_T11 (Fig. 20 A) presents just a lytic lesion and 781_T7 presents just a blastic lesion (Fig. 20 B).

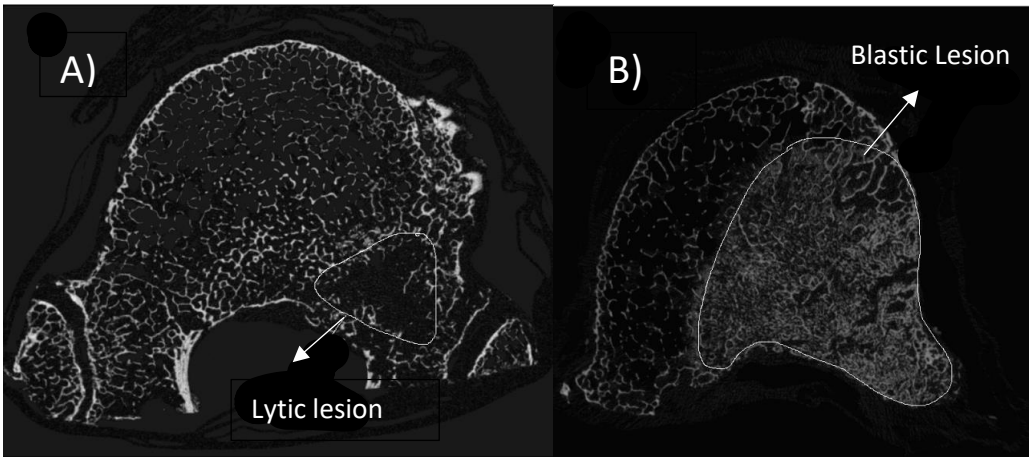

Figure 20: micro-CT scan of 772_T11 (A) and 781_T7 (B)In order to make the results clearer to the reader, a representative specimen was chosen for each type of lesion. The microstructural parameters for each representative specimen are reported (see Appendix A for the other specimens). In addition, mean values of the microstructural parameters, over the samples, are reported for each type of metastasis.

3.1.1 VERTEBRAE WITH LYTIC METASTASES

To present the microstructural results for lytic metastases, specimen 772_T6 was taken as reference (Fig. 21). The microstructural parameters were computed in correspondence of the lesion, and progressively around the lesion. Mean values of the microstructural parameters computed over the vertebrae are reported in Table 4.

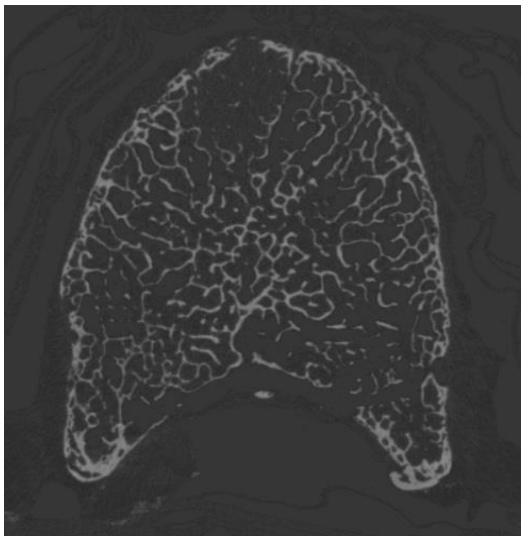

Figure 21: micro-CT scan of 772_T6

Table 4: microstructural parameter calculated in specific region in 772_T6

Masks	BV/TV [%]	Tb.Th. [um]	Tb.Sp. [um]	Tb.N. [1/mm]
772_T6_L0	0.95	107 ± 39	1505±477	0.09
772_T6_L100	9.02	156 ± 22	852±265	0.58
772_T6_L200	10.47	167 ± 21	824±255	0.63
772_T6_L300	10.99	168 ± 20	787±245	0.65
772_T6_L400	9.93	141± 19	744±236	0.70

Mean values for the whole samples are reported in Table 5 and Fig. 22.

In vertebrae affected by lytic metastases, the trend of the four microstructural parameter is similar in all the lytic samples. Minimum values for BV/TV (1.02 ± 0.04 %), Tb.Th. (128.50 ±13.04 μm) and Tb. N. (0.17± 0.2 1/mm) and maximum value for Tb. Sp. (1987.2 ± 451.69 μm) are found in correspondence of the lesion.

Table 5: mean values over the lytic samples of the microstructural parameter calculated in specific region

Masks	BV/TV[%]	Tb.Th. [um]	Tb.Sp. [um]	Tb.N. [1/mm]
L0	1.02±0.04	129±13	1987±452	0.17±0.20
L100	11.36±4.53	169±24	776±92	0.65±0.17
L200	11.70±3.94	172±24	840±52	0.66±0.15
L300	10.83±2.17	165±6	838±43	0.64±0.15
L400	11.79±4.56	158±21	773±14	0.73±0.20
L500	13.01±8.84	100 ± 57	674126	0.91±0.17

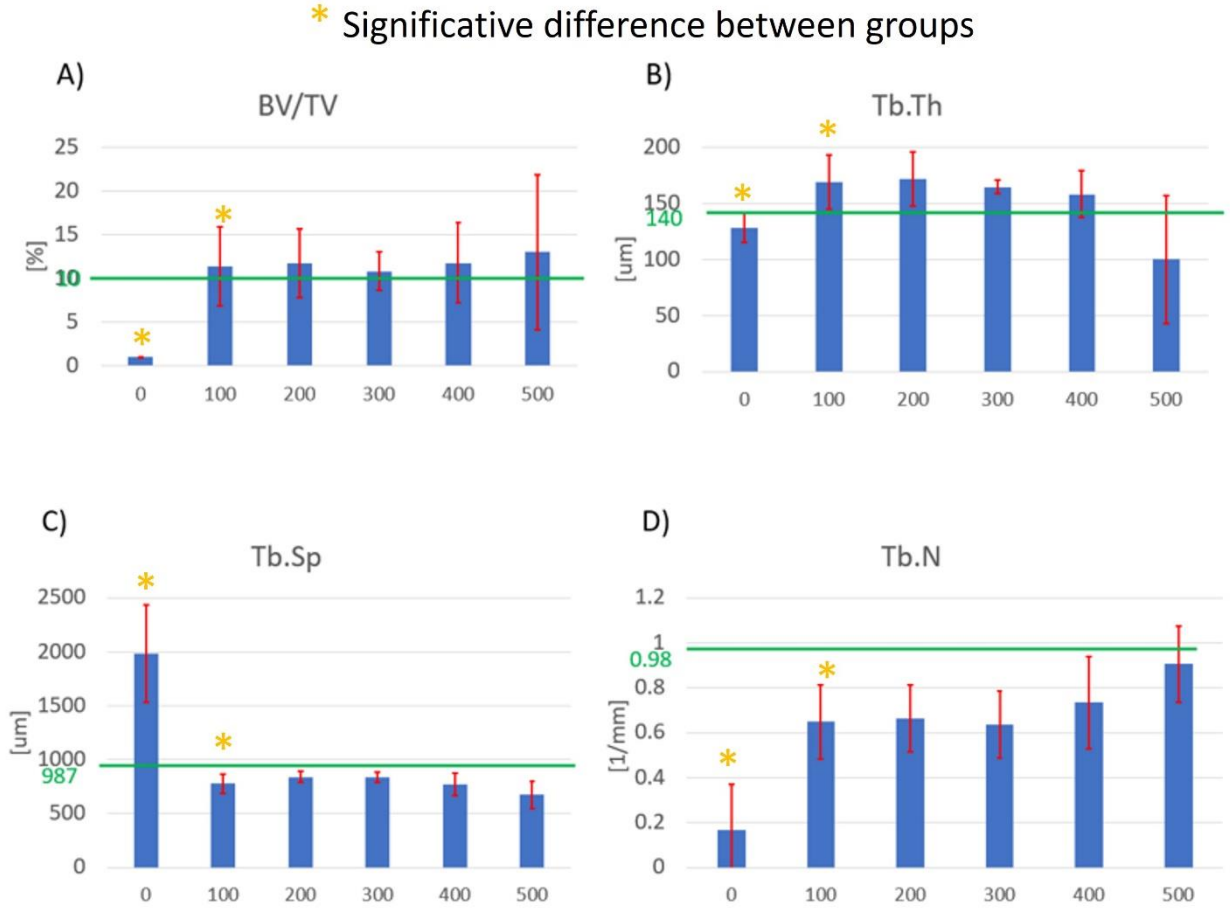

Figure 22: mean and standard deviation over the lytic samples: BV/TV (A), Tb. Th (B), Tb. Sp (C), Tb.N (D). Green lines represent the value of the parameters for healthy vertebrae reported in the literature [31

3.1.2 VERTEBRAE WITH BLASTIC LESION

In case of vertebrae with blastic lesion, specimen 777_L2 was taken as reference (Fig. 23). The microstructural parameters were computed in correspondence the lesion, inside the lesion and progressively around the lesion, till the edges of the vertebrae. Mean values of the microstructural parameters computed over the vertebrae are reported in Table 6.

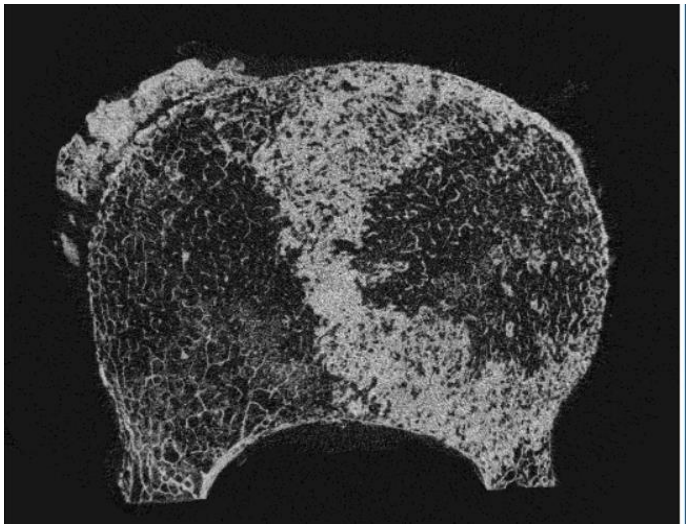

Figure 23: micro-CT scan of 777_L2

Table 6: microstructural parameter calculated in specific region in 777_L2

Masks	BV/TV [%]	Tb.Th. [um]	Tb.Sp. [um]	Tb.N.[1/mm]
777_L2_B-100	75.12	276±108	149±67	2.72
777_L2_B0	71.37	319±145	206±117	2.24
777_L2_B100	26.62	182±94	453±271	1.46
777_L2_B200	21.22	169±85	526±280	1.26
777_L2_B300	27.46	169±85	361±195	1.63
777_L2_B400	34.11	184±106	296±149	1.85

Mean values for the whole samples are reported in Table 7 and Fig. 24. In vertebrae affected by blastic metastases, the trend of microstructural parameter is similar in all blastic specimens with maximum values for BV/TV (75.12 %), Tb.Th. (275.96

µm) and Tb. N. (2.72 1/mm) and minimum values for Tb. Sp (149.37 µm) inside the lesion.

Table 7: mean values over the blastic samples of the microstructural parameter calculated in specific region

Masks	BV/TV [%]	Tb.Th. [um]	Tb.Sp. [um]	Tb.N. [1/mm]
B-100	75.12	276	149	2.72
B0	58.52±2.29	267±18.17	262±80	2.18±0.45
B100	20.03±15.63	180±9.32	356±356	1.11± 0.31
B200	16.02±13.64	174±7.35	305±305	0.93± 0.27
B300	27.46	169	361	1.63
B400	34.10	184.12	296.16	1.85

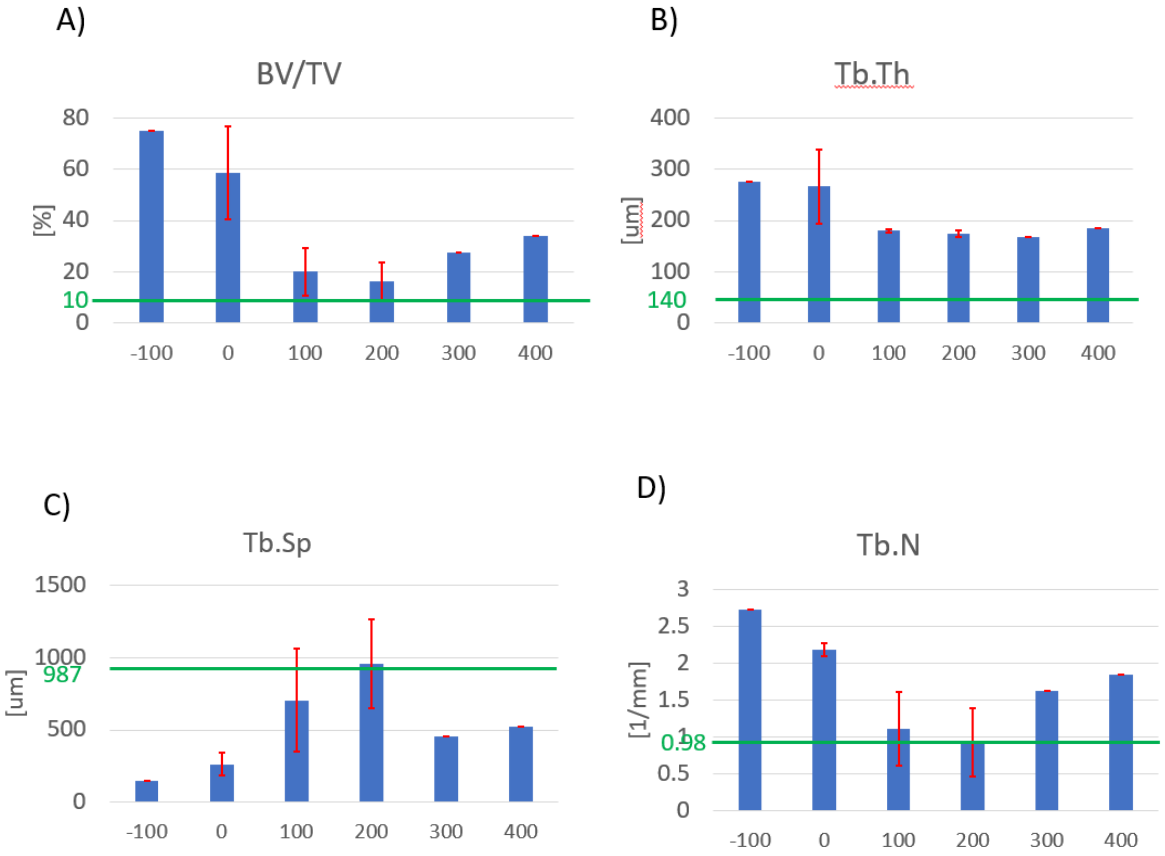

Figure 24: mean and standard deviation over the blastic samples: BV/TV (A), Tb. Th (B), Tb. Sp (C), Tb.N (D). Green lines represent the value of the parameter fort healthy vertebrae reported in literature [31].

3.1.3 VERTEBRAE WITH MIXED LESION

As mixed metastases are characterized by the presence of both lytic and blastic metastases, the microstructural analysis was performed for both lesions. In case of vertebrae with mixed metastases, specimen 771_T12 was taken as reference (Fig. 25). Results from the microstructural analysis focused on the lytic part are reported in Table 8, the ones focused on the blastic part are reported in Table 9.

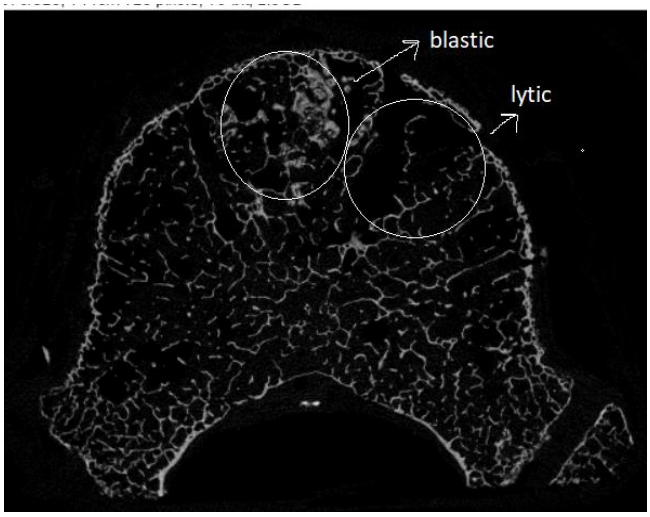

Figure 25: micro-CT scan of 771_T12

Table 8: microstructural parameter calculated in specific region in 771_T12, lytic portion

Masks	BV/TV [%]	Tb.Th. [um]	Tb.Sp. [um]	Tb.N. [1/mm]
771_T12_L0	1.74	141±47	2427±1331	0.12
771_T12_L100	7.41	166±66	1107±471	0.45
771_T12_L200	6.75	161±59	1134±525	0.42
771_T12_L300	8.60	171±65	956±398	0.50
771_T12_L400	8.93	181±77	952±408	0.49
771_T12_L500	10.49	173±66	885±362	0.61
771_T12_L600	11.14	169±65	885±433	0.66
771_T12_L700	12.42	163±62	777±345	0.76

Table 9: microstructural parameter calculated in specific region in 771_T12, blastic portion

Masks	BV/TV[%]	Tb.Th. [um]	Tb.Sp. [um]	Tb.N.[1/mm]
771_T12_B-100	17.99	202±99	554±265	0.89
771_T12_B0	21.93	244±126	686±373	0.90
771_T12_B100	13.24	188±81	709±358	0.70
771_T12_B200	12.83	189±82	729±384	0.68

771_T12_B300	13.18	200±93	763±369	0.66
771_T12_B400	11.64	181±76	804±378	0.64
771_T12_B500	12.42	163±65	702±303	0.76
771_T12_B600	15.59	158±64	543±235	0.99

Regarding the mean values over the mixed samples, the microstructural analysis was performed both in masks of lytic and blastic lesions and surrounding these areas. Firstly, the mean values have been calculated considering just one of the lesions and are reported in two different tables considering the type of metastasis, lytic lesion in Table 10 and blastic lesion in Table 11. The trend of the four parameters for both lytic and blastic lesion is reported in Fig. 26 and was found similar to the trend of vertebrae affected by lytic and blastic metastases. Indeed, BV/TV (5.36 ± 2.89 %), Tb.Th. (157.24 ± 49.47 μm) and Tb. N. (0.38 ± 0.26 1/mm) reached minimum values and Tb. Sp. (1398.38 ± 970.58 μm) reached maximum value in correspondence of the lytic lesion. Whereas, BV/TV (59.92 ± 38.36 %), Tb.Th. (289.76 ± 98.86 μm) and Tb. N. (2.08 ± 1.07 1/mm) reached maximum values and Tb. Sp. (305.07 ± 232.98 μm) reached minimum value inside or in correspondence of the blastic lesion.

Table 10: mean values over the lytic part of the mixed samples of the microstructural parameter calculated in specific region

Masks	**BV/TV [%]**	**Tb.Th. [um]**	**Tb.Sp. [um]**	**Tb.N. [1/mm]**
L0	5.36±2.89	157±49	1398±91	0.38±0.26
L100	15.27±11.01	218±85	779 ±226	0.65±0.20
L200	12.88±9.25	195±55	832±237	0.61±0.24
L300	13.41±8.34	198±43	801±179	0.64±0.24
L400	12.70±7.37	185±20	785±17	0.66±0.30
L500	15.66±6.91	192±24	770±157	0.80±0.27
L600	13.61±3.67	197±49	821±127	0.69±0.02
L700	9.68±3.88	156±10	861±120	0.61±0.21

Table 11: mean values over the blastic part of the mixed samples of the microstructural parameters calculated in specific region

Masks	**BV/TV [%]**	**Tb.Th. [um]**	**Tb.Sp. [um]**	**Tb.N. [1/mm]**

B-100	59.92±38.36	274±99	305±233	2.08±1.07
B0	53.88±22.36	290±46	435±219	1.83± 0.16
B100	14.26±6.52	195±44	796±133	0.71±0.15
B200	13.27±5.29	200±40	827±150	0.65±0.16
B300	16.20±7.02	24489	858±169	0.66±0.17
B400	17.88±12.07	220±76	795±208	0.76±0.24
B500	15.41±3.49	175±12	689±144	0.88±0.19
B600	16.96±1.27	15636	448±257	1.14±0.34

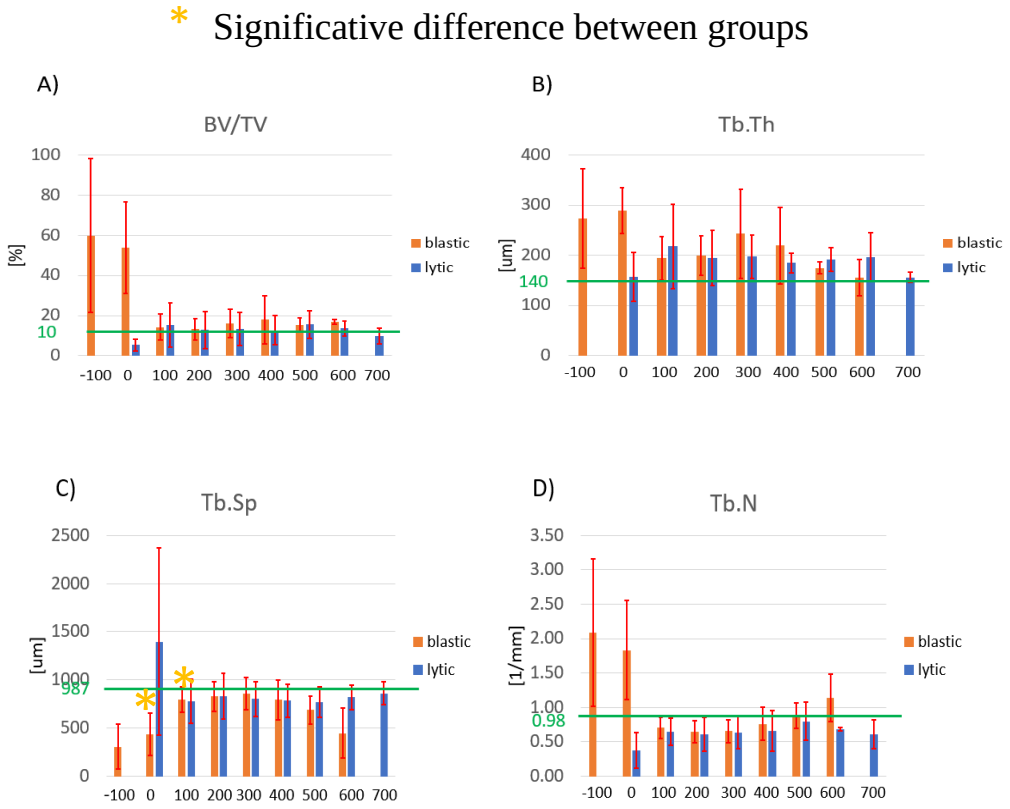

Figure 26: mean and standard deviation over the mixed samples: BV/TV (A), Tb. Th (B), Tb. Sp (C), Tb.N (D). Green lines represent the value of the parameter for healthy vertebrae reported in literature [31]

3.1.4 STATISTICAL ANALYSIS

The statistical analysis of the microstructural analysis was performed to evaluate if there were statistically significant differences in the microstructural parameters among areas close and far from the lesion. The analysis was computed for each group of metastatic

vertebrae. In case of lytic metastases, statistically significative differences were found between the lytic lesion and the surrounding tissue (p-value < 0.001) in all the microstructural parameters (BV/TV, Tb. Th, Tb. Sp, Tb. N.). No statistically significative differences in the microstructural parameters were found among regions surrounding the lesion.

In case of blastic metastases, no statistically significative differences were found between the blastic lesion and the surrounding tissue, between the blastic lesion and the shrinkage of the lesion and among areas surrounding the lesion in all the microstructural parameters (BV/TV, Tb. Th., Tb. Sp., Tb. N.).

Finally, in case of mixed metastases, a statistically significative difference was found in Tb. Sp. between the blastic lesion and the surrounding tissue. No statistically significative differences were found among areas surrounding the lesion for both lytic and mixed lesion in all the microstructural parameters (BV/TV, Tb. Th., Tb. Sp., Tb. N.).

3.2 MECHANICAL ANALYSIS

The mechanical analysis was computed in the same specific areas used previously for the microstructural analysis. The internal strain field was computed with a global DVC approach, called BoneDVC and the 3D color map was evaluated by ANSYS to visualize the internal strain field. As for the microstructural analysis, a representative specimen, the same chosen previously to represent the microstructural results, was chosen for every metastatic group.

3.2.1 VERTEBRAE WITH LYTIC METASTATASES

To present the mechanical results for lytic metastases, specimen 772_T6 was taken as reference. The 3D strain color map and mean values of minimum principal strains (ε3), computed for every region of interest are reported in Fig 27 and Table 12 respectively. Mean values for the whole samples are reported in Table 13 and Fig. 28.

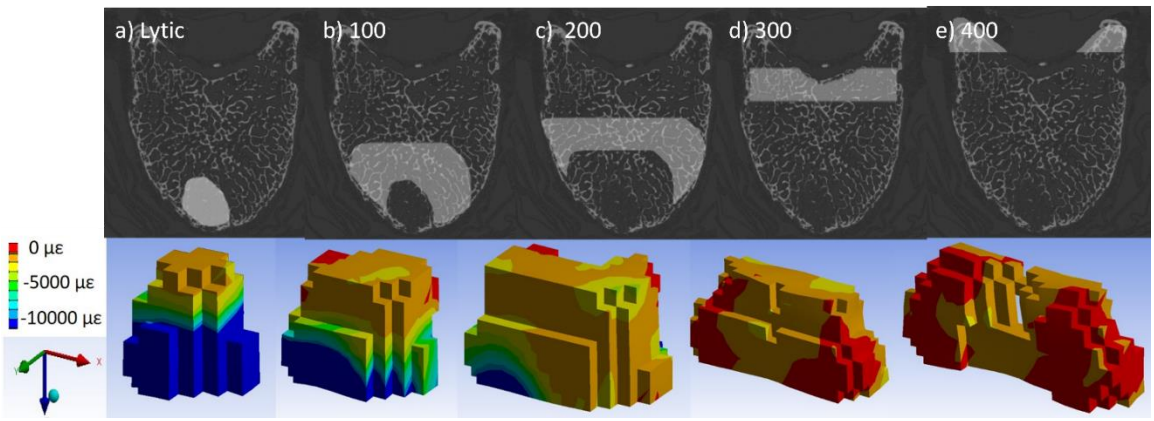

Figure 27: 3D strain colour map computed in every ROIs in 772_T6. Larger values of ε3 are reported in blue and smaller values in red .

Table 12: Mean and Standard Deviation of ε3 calculated in specific regions of 772_T6

Masks	**ε3 (με)**
L0	-22672± 17981
L100	-14945± 16483
L200	-8307±11310
L300	-1932±1249
L400	-1419± 611

Table 13: Mean and Standard Deviation of ε3 calculated in specific regions over the lytic samples

Masks	**ε3 (με)**
L0	-12800±8017
L100	-11127±9128
L200	-9569±8932
L300	-7813±8515
L400	-6301±6508
L500	-8045±7765

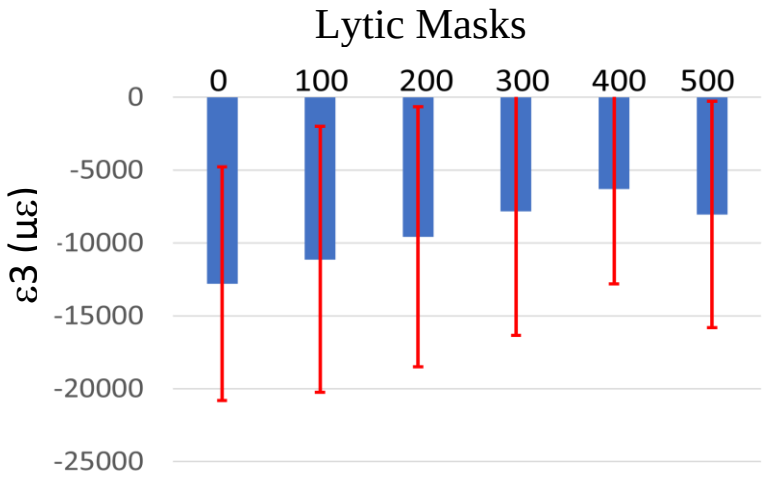

Figure 28: media and standard deviation over the lytic samples

Mechanical results over all the lytic samples showed that larger minimum principal strains are reached in correspondence of the lesion. In particular, larger values are found in correspondence of the lytic metastases in all specimens except for specimen 772_T11 (larger value is present in L500) and 772_L4 (larger value is present in L100). In addition, in specimen 772_L4 lower minimum principal strains were found in the area furthest from the lesion, which corresponded to the pedicles.

3.2.2 VERTEBRAE WITH BLASTIC METASTASES

To present the mechanical results for mixed metastases, specimen 777_L2 was taken as reference. Mechanical results on lytic lesion are reported in Table 14 and Fig. 29, while mechanical results on blastic lesion are reported in Table 15 and Fig. 30. Mechanical results over all the blastic samples showed that larger minimum principal strains are present in regions far from the lesion, wherease the regions correspondent to the lesion present lower strains.

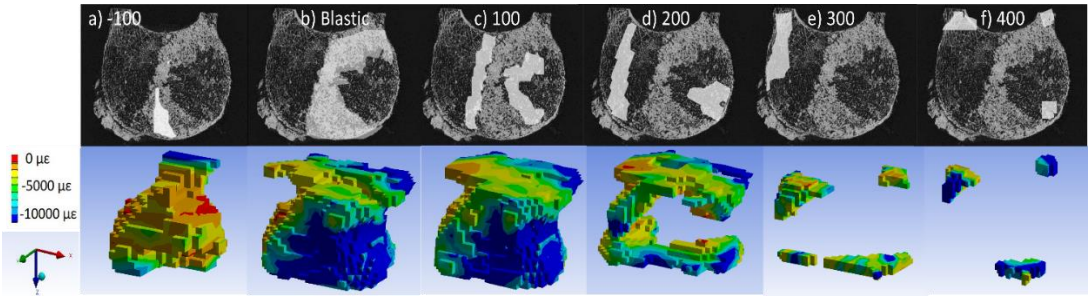

Figure 29: 3D strain colour map computed of 777_L2. Larger values of e3 are in blue and smaller values in red

Table 14: Mean and Standard Deviation of ε3 calculated in specific regions of 772_L2

Masks	ε3 (με)
B-100	-3531± 2374
B0	-4408± 2567
B100	-4092± 2577
B200	-3708± 2447
B300	-6802± 3387
B400	-7760± 4074

Table 15: Mean and Standard Deviation of ε3 calculated in specific regions over the blastic samples

Masks	ε3 (με)
B-100	-3531± 2374
B0	-7270±3944
B100	-6685±3971
B200	-5472±3480
B300	-6802±3387
B400	-7759±4074

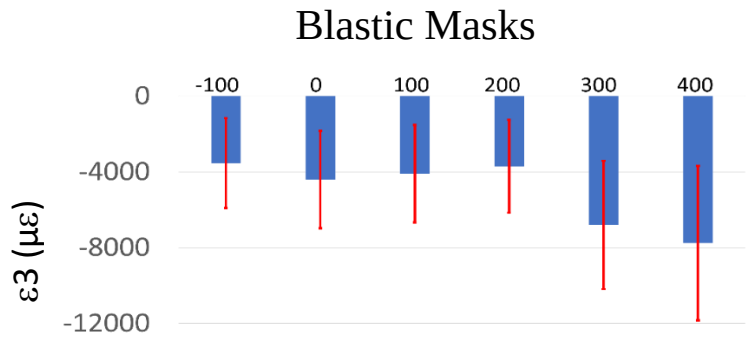

Figure 30: media and standard deviation over the blastic samples

3.2.2 VERTEBRAE WITH MIXED METASTATASES

To present the mechanical results for mixed metastases, specimen 771_T12 was taken as reference. Mechanical results on lytic lesion are reported in Table 16 and Fig. 31, while mechanical results on blastic lesion are reported in Table 17 and Fig 32.

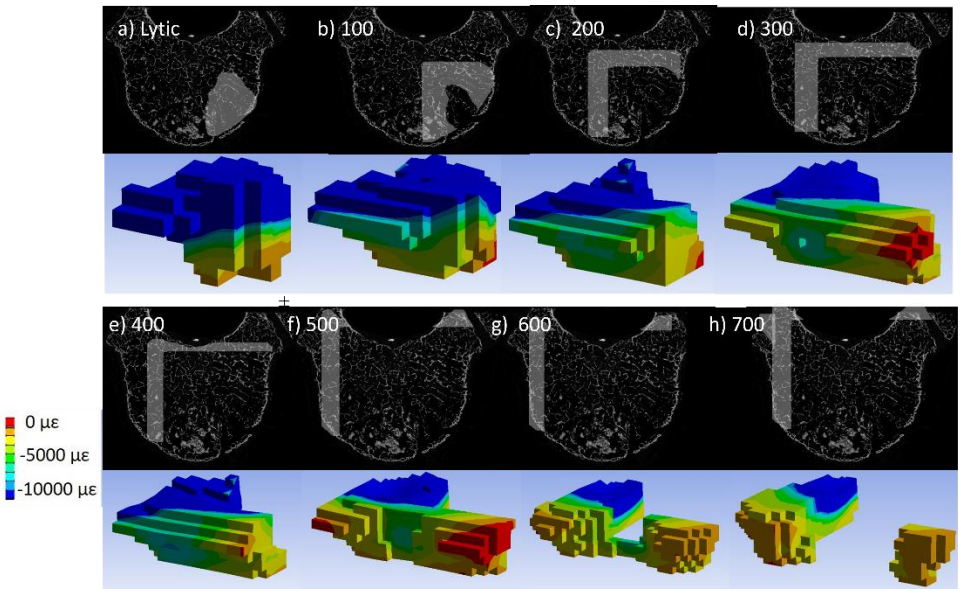

Figure 31: 3D strain colour map computed in lytic part of 771_T12. Higher values of e3 are in blue and lower values in red

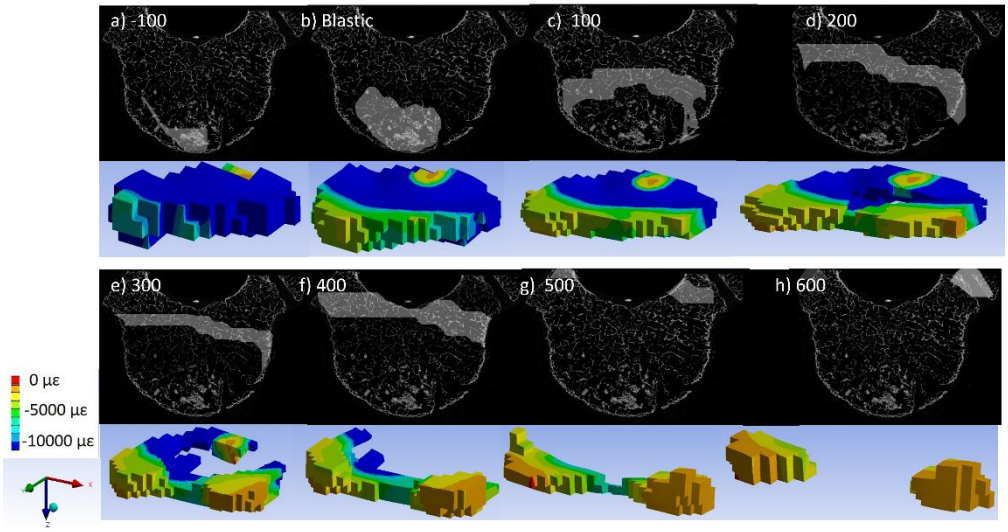

Figure 32: 3D strain color map computed in blastic part in 771_T12. Higher values of e3 are in blue and lower values in red

Table 16: Mean and Standard Deviation of ε3 calculated in specific region in 771_T12, regarding lytic part

Masks	ε3 (με)
L0	-20208±15212
L100	-16623±14603
L200	-13351±11555
L300	-13298±11630

L400	-10967±11799
L500	-8316±10303
L600	-6696±11078

Table 17: Mean and Standard Deviation of ε3 calculated in specific region in 771_T12, regarding lytic part

Masks	ε3 (με)
B-100	-26615±14121
B0	-20882±14922
B100	-16788±14534
B200	-15747±15302
B300	-11666±13585
B400	-5372±5800
B500	-2768±2259
B600	-13201±978

Mean values for the lytic part over the samples are reported in Table 18. Mean values for the blastic part over the samples are reported in Table 19. The trend of e3 for both lytic and blastic lesion is reported in Fig. 33.

Table 18: Mean and Standard Deviation of ε3 over the lytic part of the mixed samples

Masks	ε3(με)
L0	-7424±4917
L100	-6740±5018
L200	-5831±4416
L300	-5806±4548
L400	-5353±4861
L500	-4964±5018
L600	-5626±6702
L700	-5046±7412

Table 19: Mean and Standard Deviation of ε3 over the blastic part of the mixed samples

Masks	ε3 (με)

B-100	-10953±5874
B0	-7510±5086
B100	-6664±5179
B200	-6590±5972
B300	-6196±6482
B400	-3943±3433
B500	-2882±2250
B600	-2630±1760

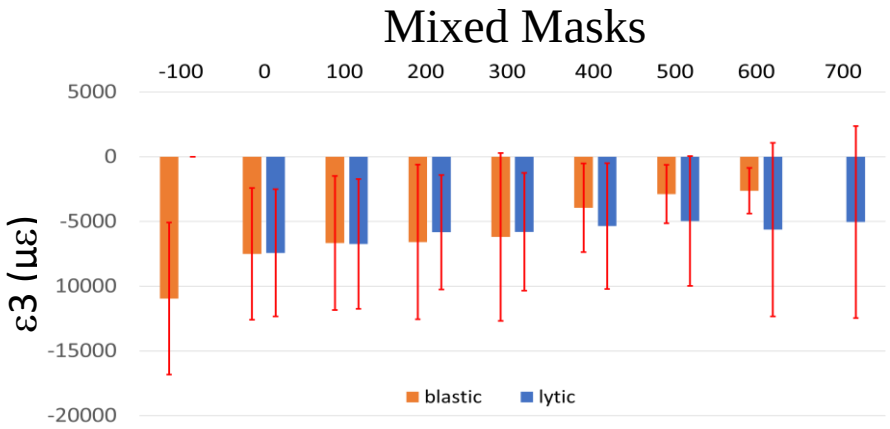

Figure 33: media and standard deviation over the mixed samples

Mechanical results on mixed metastases highlight the heterogeneity of the strain distribution. Considering only the lytic part of the mixed metastases, in two specimens (771_T12 and 780_T6) larger minimum principal strains were found in correspondence of the lesion, as previously observed in case of vertebrae affected by lytic metastases and lower minimum principal strains were found in the area furthest from the lesion, which corresponded to the pedicles. Other two specimens (776_L4 and 781_T12) reached larger minimum principal strains far from the lytic lesion (L600) and lower minimum principal strains were found in correspondence of the lesion. Whereases, considering only the blastic part of the mixed metastases, the area corresponding to the blastic lesion reached lower minimum principal strains, while larger minimum principal strains were found in the furthest areas (pedicles), as previously observed in case of blastic metastases. In only one specimen (771_T12) larger minimum principal strains were found in correspondence and inside the lesion and lower minimum principal strains were found in the furthest area (pedicles).

3.3 CORRELATION AMONG MICROSTRUCTURAL PARAMETERS AND MECHANICAL BEHAVIOUR

The statistical correlations were performed for each metastatic group to evaluate if there is an influence among the microstructural pattern and the mechanical behaviour. Significative positive and weak correlations were found in lytic metastases for BV/TV (R^2=0.2) (Fig. 34 A), Tb. Th. (R^2=0.23) (Fig. 34 B) and Tb. N. (R^2=0.17) (Fig. 34 D). No significative agreement was found in lytic metastases for Tb. Sp. (R^2=0.02) (Fig. 34 C).

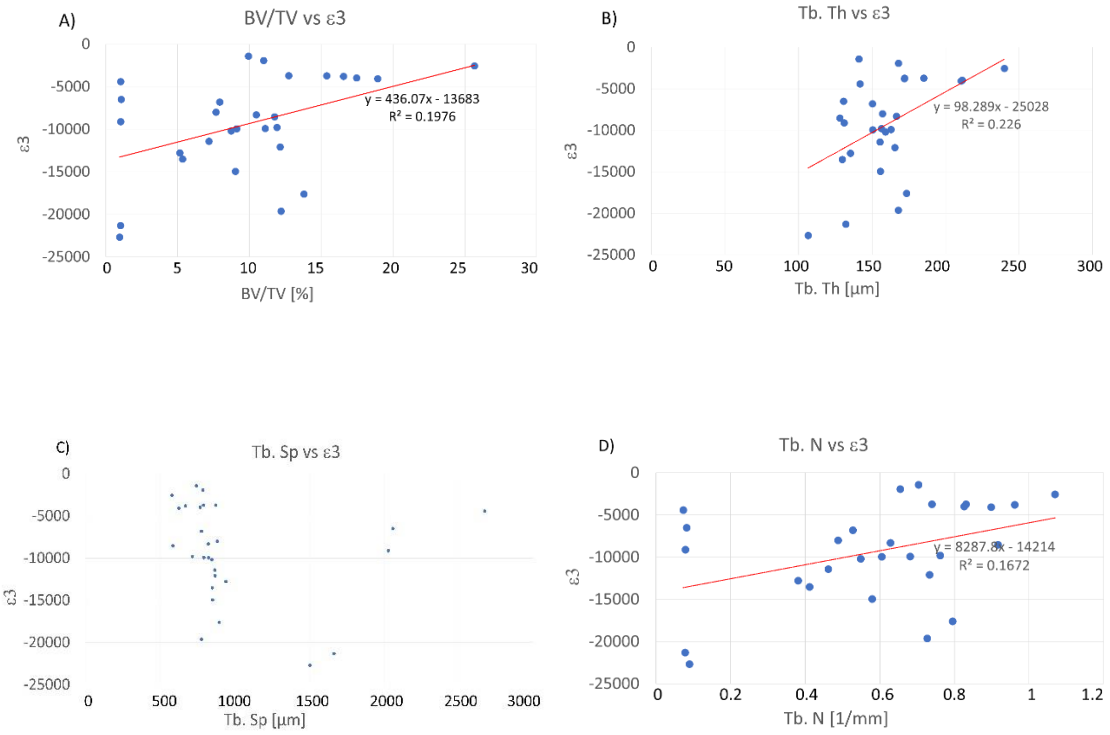

Figure 34: correlation between BV/TV and ε3 (A), Tb. Th. and ε3 (B), Tb. Sp. and ε3 (C), Tb. N. and ε3 (D) in lytic metastases

No significative agreement was found in blastic metastases for BV/TV (R^2=0.04) (Fig. 35 A), Tb. Th. (R^2=0.012) (Fig. 35 B), Tb. Sp. (R^2=0.31) (Fig. 35 C) and Tb. N. (R^2=0.094) (Fig. 35 D).

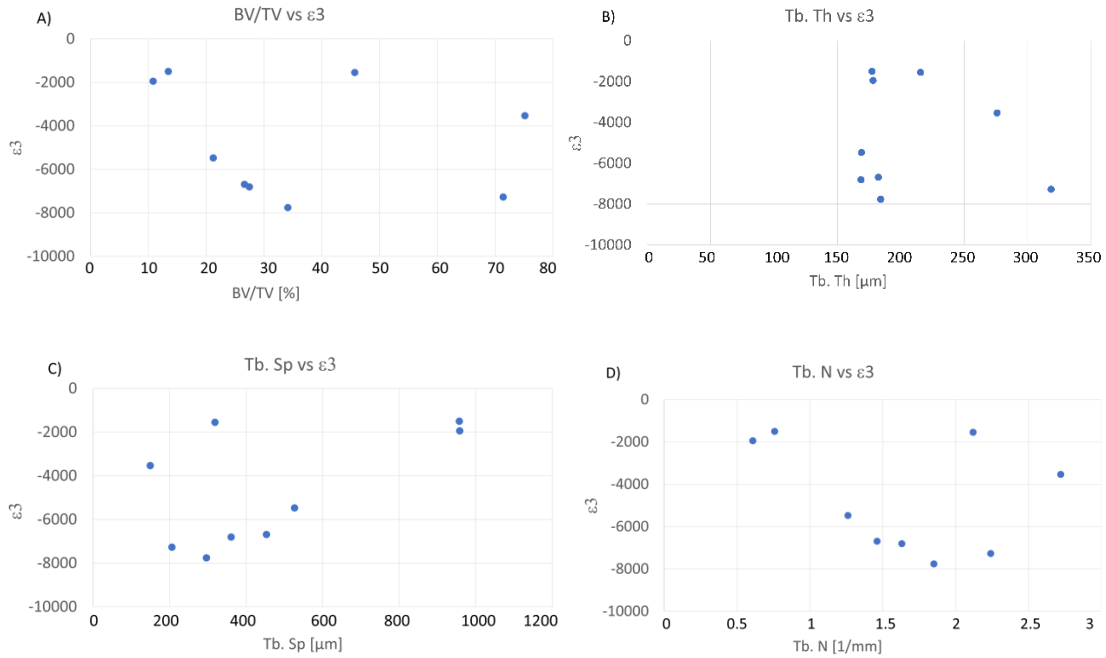

Figure 35: correlation between BV/TV and ε3 (A), Tb. Th. and ε3 (B), Tb. Sp. and ε3 (C), Tb. N. and ε3 (D) in blastic metastases

Significative positive correlation was found in mixed metastases for Tb. Th. (R^2=0.096) (Fig. 36 B). No significative agreement was found in mixed metastases for BV/TV (R^2=0.04) (Fig. 36 A), Tb. Sp. (R^2=0.013) (Fig. 36 C) and Tb. N. (R^2=0.05) (Fig. 36 D).

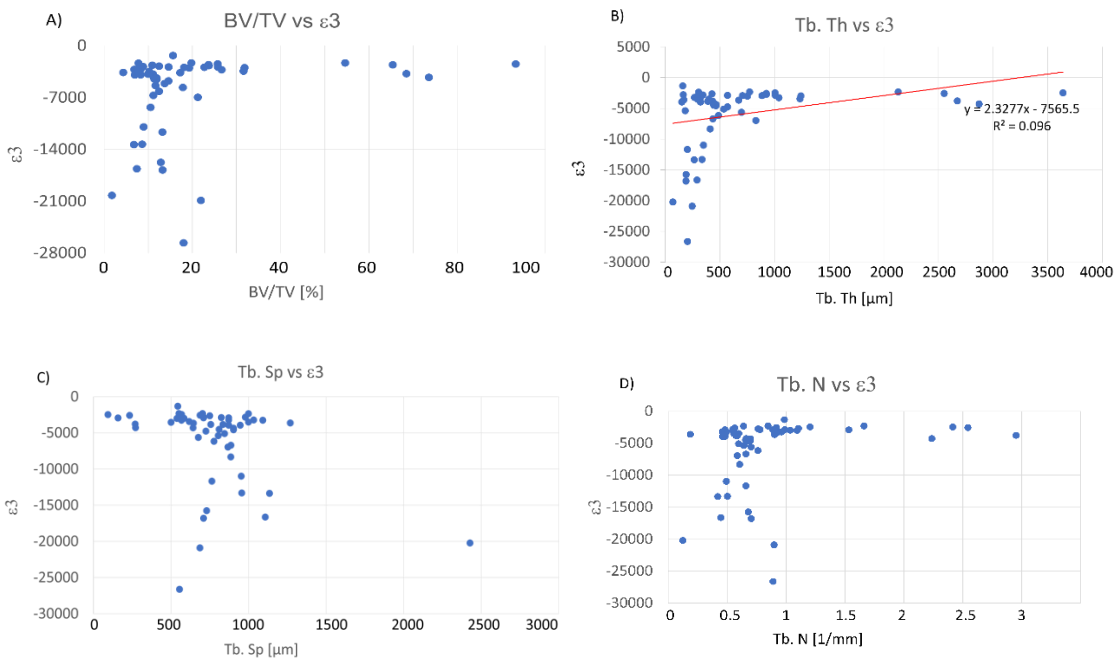

Figure 36: correlation between BV/TV and e3 (A), Tb. Th. and e3 (B), Tb. Sp. and ε3 (C), Tb. N. and ε3 (D) in mixed metastases

Considering all metastatic vertebrae, Significative positive correlations were found in BV/TV (R^2=0.07), Th. (R^2=0.09) and Tb. N. (R^2=0.086) (Fig. 34 D). No significative agreement was found for Tb. Sp. (R^2=0.07).

CHAPTER 4: DISCUSSION

The aim of this study was to evaluate the effect of the microstructural features on the mechanical properties of human metastatic vertebrae by measuring the correlation between the 3D strain field inside the vertebrae and the microstructural parameters. In particular, the microstructural analysis on the micro-CT images was performed in specific regions of interest: near, far and within the lesions. The internal strain field in metastatic vertebrae, tested in pure compression until failure, was measured using a global DVC, called BoneDVC, in the same specific regions of interest.

To date, to the author's knowledge, the characterization of metastatic vertebrae has partially been studied but there is still a lack of characterization in the microstructural and mechanical properties of metastatic spine. Regarding the effects of the presence of the metastases on the microstructure, lytic metastases in rat vertebrae [28] lead to a reduction in Tb. N, Tb. Th. and blastic metastases in human lumbar vertebrae lead to an increase in BV/TV and Tb. N., without significative changes in Tb. Th. As regarding the assessment of the mechanical behaviour of the spine in 2020, Palanca et al [11] demonstrated how artificial lesions to simulate lytic defects reduce strength and loads bearing of porcine vertebrae. Other studies [12] [13] have demonstrated that vertebrae affected by lytic metastases reached larger strain than healthy ones. By contrast, blastic and mixed metastases didn't show a univocal trend [13] in fact sometimes the larger strains were found in metastatic vertebrae and in other cases, in healthy vertebrae.

In this study, the microstructural and mechanical analysis of human metastatic vertebrae was performed in specific ROIs starting from the lesion and to enlargement and shrinkages of the lesion itself. Results showed three different behaviours, both in the microstructural and mechanical investigation. These different trends depend on the effects of the different types of metastases: lytic, blastic and mixed. In case of vertebrae affected by lytic metastases, in the area involved with the lesion there are alterations of the microstructural features and larger strains. In case of vertebrae with blastic metastastis, in the area involved with the lesion there are alterations in the microstructural pattern and smaller strains. Vertebrae with mixed metastases present characteristics in between for both the microstructural and mechanical features. Vertebrae affected by lytic metastases showed a similar trend in all the specimens, regarding both the microstructural and mechanical analysis. Indeed, in presence of the lesion, there is a reduction in BV/TV, Tb. Th. and Tb. N. and an increase in Tb. Sp. in correspondence of the lesion, in comparison

with the data of healthy vertebrae present in literature [31]. These changing in the microstructural features reflect the lack of portion of bone tissue, which is typical of lytic metastases. Indeed, lytic metastases present lacks in the bone tissue, due to the bone reabsorption process. Consequently, regions including the compromised microstructure due to the presence of the lytic lesion seem to be weaker and more likely to reach larger strain and compromising the load bearing capacity and instability of the spine. However, statistical analysis showed low correlation between the internal strain field and the microstructural features. Moreover, spine is usually subjected to different loads in fact the bone structure is optimized to equally distribute, bear and transfer loads. For this reason, the lack of bone tissue was expected to encourage an optimization of the bone tissue in regions close to the lytic metastases. However, regions surrounding the lytic lesion have microstructural features similar to those present in healthy vertebrae [31]. These results support the previous hypothesis about the local influence of the metastases on the vertebral tissue. Indeed, statistical results on lytic metastases may lead to the assumption that the tissue surrounding the lytic lesion can be considered as healthy tissue. In addition, an increase in BV/TV and Tb. N. and a reduction in Tb. Sp. was found in the posterior areas of the vertebrae (coherent with the results of Perilli et al. regarding the heterogeneity of the vertebral tissue [32]). One rationale thinking of the increase of BV/TV is that the posterior areas are constituted by posterior elements with a larger portion of cortical tissue, denser than trabecular tissue, to reinforce and protect to the central vertebral body, mainly constituted by trabecular structure [31]. As for vertebrae with lytic metastases, a unique trend was found for vertebrae with blastic metastases. In correspondence of the lesion, there is an alteration of the microstructural features with higher values of BV/TV, Tb. Th. and Tb. N. and lower value for Tb. Sp. in comparison with the data of healthy vertebrae present in literature [31]. These results show the peculiar characteristic of the blastic tissue: the growth and thickening of the bone tissue in correspondence of the lesion. These results showed how blastic metastases are characterized by a denser portion of bone tissue that reached lower strains than those of the regions far from the lesion. Indeed, the areas of the vertebral body far from the blastic lesion do not present alterations in the microstructure and larger strains are reached. In fact, mechanical failure can occur in the metastatic vertebra in region far from the lesion or even in the adjacent healthy vertebrae, as previously observed in another study [13] where in some cases control vertebrae reached larger strains that the vertebra with blastic metastases.

In case of vertebrae affected by mixed metastases, we observed two different microstructural and mechanical trends for the lytic and blastic lesions.

Mechanical results on vertebrae affected by mixed metastases highlight the heterogeneity of the strain distribution. Indeed, in vertebrae with mixed metastases with a predominance of the blastic lesion over the lytic lesion (Fig. 37), the mechanical behaviour was similar to one of vertebrae affected by blastic metastases and in case of predominance of lytic lesion the mechanical behaviour was found similar to the one of vertebrae affected by lytic metastases. Further analysis may find a rationale between the lesions, to evaluate if a vertebra affected by mixed metastases have a mechanical behaviour similar to blastic or lytic vertebrae.

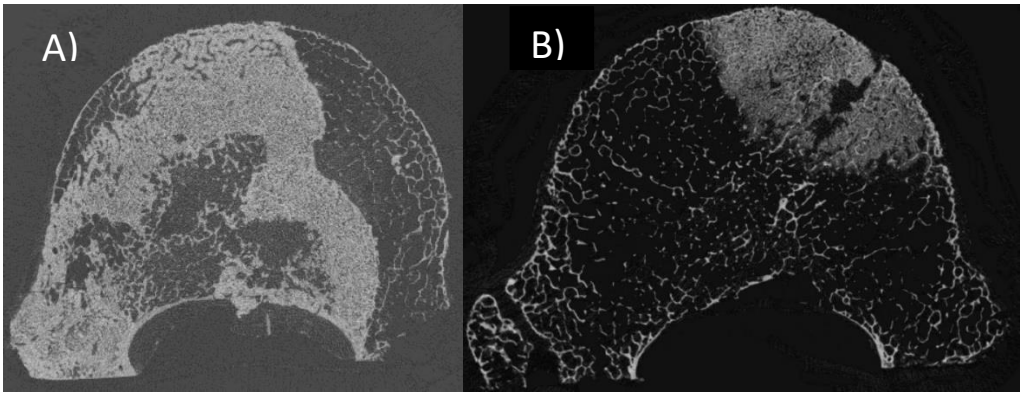

Figure 38: microCT scan of 776_L4 (A) and 781_T12 (B)

However, some limitations must be taken into account. First of all, the small sample size does not permit to generalise these findings. Indeed, the statistical analyses performed on blastic (2) and mixed (4) specimens are not reliable due to the small number of specimens analysed. Future analysis on a larger sample size is required to validate the findings.

In addition, all specimens were obtained from cadavers with different characteristics such as weight, age, height, lifestyle and eventually pharmacological treatment to alleviate symptoms. Indeed, further analysis should be carried out to evaluate if anti-tumoral drugs may have an influence on the microstructural pattern of the vertebral tissue.

The microstructural analysis was performed only in metastatic vertebrae, even if all the specimens consisted in spine segment with a metastatic and a healthy vertebra in the middle. However, to compare metastatic and healthy vertebrae data from the literature were used and not control data. Next steps in future analysis should involve the study of the microstructural pattern in control vertebrae and the comparison with data from metastatic vertebrae, obtained in this study.In addition, to evaluate the microstructural pattern, only

the parameters most reported in literature have been chosen, however, the microstructural investigation could be easily extended to other parameters.

Moreover, each metastatic samples presented variability in the metastatic features such as position, dimension and type. In this study, metastatic vertebrae were classified only for type. In the future, position should be taken into account, especially in vertebrae affected by mixed metastases where the position between the two lesions was not considered and some masks of the lesion may include part of other lesion mask.

As regarding the image processing phase, it was performed starting from the images of a previous study. A manual segmentation of the micro-CT images to select the portion affected by the metastases was manually performed and all the masks preparation process was operator dependent. In addition, the masks had the limit to be bidimensional and the image processing phase is a time-consuming process.

CONCLUSIONS

In this work, for the first time, the microstructural pattern was evaluated to study the effect of metastases in specific regions in human metastatic vertebrae. In addition, the internal strain field was measured in the same regions of interest to study the mechanical behaviour at failure. The internal strain field was computed using a Digital Volume Correlation (DVC) approach called BoneDVC.

The outcomes of the microstructural analysis revealed the different changing in the microstructure of the vertebrae due to the presence of different types of metastases, in comparison with literature data. Results from the mechanical and microstructural characterization highlight the presence of two different trend. In case of vertebrae with lytic lesions the presence of the metastases influences the microstructural pattern only in the area affected by the lesion, characterized by a lack of the vertebral tissue. As a consequence, the mechanical behaviour reflects the microstructure, in fact the region including the lytic lesion, reached larger strains and seemed to be weaker and more likely to increase the stability of the spine. In case of vertebrae affected by blastic lesions there is an alteration of the microstructure in correspondence of the lesion, where there is a denser portion of tissue. In this case, the regions including the blastic metastases reached lower strains and seemed to be stiffer with a higher resistance to loads-bearings. In addition, both for vertebrae affected by lytic and blastic lesions, the microstructural patter in regions surrounding the lesion is similar to that of healthy vertebrae.

These results suggest the local impact of bone metastases on the vertebral tissue. Finally, vertebrae with mixed metastases, that are constituted by both blastic and lytic metastases, present aspects in common. The microstructural features are altered in both regions corresponded to the lesion with the same trend of vertebrae affected by lytic and blastic lesion. However, result of the mechanical analysis do not show a systematic trend. The mechanical behaviour seems to be influence by the proportion of the two lesions, as vertebrae with mixed lesion with a blastic predominance over the lytic metastases present an internal strain distribution similar to vertebrae affected by blastic metastases. Further analysis should be carried out to find a useful ratio between the lesions to evaluate whether or not a vertebra affected by mixed metastases present a predominant lytic/blastic mechanical behaviour. Moreover, in case of vertebrae with mixed metastases, the position of the metastases should be taken into account to consider if there is an influence between the two lesions and evaluate the loads and microstructural distribution proportional to the

lesions. Another aspect to be study in the future is the evaluation of the possible fracture location and the and the modality of fracture in the different types of metastatic vertebrae (lytic, blastic and mixed). Finally, future analysis on the nature of the blastic tissue may help to evaluate the optimization and calcification of the blastic tissue and if the quality/quantity have a role in the loads-bearings resistance.

This regional study permitted to evaluate the distribution of the microstructural features in different region of vertebrae affected by different types of metastases (lytic, blastic and mixed). In addition, the local analysis of the microstructural and mechanical assessment permitted to evaluate the possible influence of the microstructural architecture on the loads-bearing capacity and mechanical stability of the spine.

ACKNOWLEDGEMENTS

Firstly, I would like to thank Prof. Luca Cristofolini for giving me the opportunity to take part in this research. I would like to thank Marco Palanca. He really contaminated me with his passion for research. One think that struck me the most was that he treated me not like a simple student, but like a member of the team. One think that taught me was to always ask questions and interrogate myself without doing only my "compitino". I promise you I will read "Il conte di Montecristo" one day or another.

And Giulia is the person I would like to thank the most. I really enjoyed working with you and I do not think that my work would be the same without your help. I really really thank you for helping me, especially with technical problems (all the times that programs did not run, you always had a solution!) and for always be there to help me even if you were occupied or hit by bad luck. Sincerely, I never met anyone who were hit by so many unlucky events in just few months as you.

Finally, I want to thank all the people that shared all these years with me. Starting from my family, who always supported and trusted me. Thanks goes to my grandfather who raised me and congratulated with me for getting my degree on 30 of August because he misunderstood the date, to my parents who always were so patient with me, even if I am very messy (sorry mom for all the times you said to me to tidy up my room and I pretended to not hear you) and I lost all my documents twice in just a month. The person I would like to thank the most is my sister Chiara. Thank you for always be there for me. You make me laugh like no one else does and I will miss you so much, especially all the gossip that we do. Thank you WIFI connection for being unexpectedly so stable, on the contrary of my mind, during my online exams.

In the end I want to thank all my friends, especially Marghe, Lalla and Ami. You supported me and listened to all my "scleri", giving me advice without complaining. Thank you for all the "serate" that we shared together. You were always by my side and I know you will always be.

BIBLIOGRAPHY

[1] T. Skrinskas, M. Clemons, O. Freedman, I. Weller, e C. M. Whyne, «Automated CT-based analysis to detect changes in the prevalence of lytic bone metastases from breast cancer», *Clin Exp Metastasis*, vol. 26, n. 2, pagg. 97–103, feb. 2009, doi: 10.1007/s10585-008-9219-6.

[2] R. G. David, «Mechanisms of Bone Metastasis», *The New England Journal of Medicine*, pag. 10, 2004.

[3] M. Palanca *et al.*, «Type, size, and position of metastatic lesions explain the deformation of the vertebrae under complex loading conditions», *Bone*, vol. 151, pag. 116028, ott. 2021, doi: 10.1016/j.bone.2021.116028.

[4] I. Laufer *et al.*, «The NOMS framework: approach to the treatment of spinal metastatic tumors», *Oncologist*, vol. 18, n. 6, pagg. 744–751, giu. 2013, doi: 10.1634/theoncologist.2012-0293.

[5] C. G. Fisher *et al.*, «A Novel Classification System for Spinal Instability in Neoplastic Disease: An Evidence-Based Approach and Expert Consensus From the Spine Oncology Study Group», *Spine*, vol. 35, n. 22, pagg. E1221–E1229, ott. 2010, doi: 10.1097/BRS.0b013e3181e16ae2.

[6] A. L. Versteeg *et al.*, «The Effect of Introducing the Spinal Instability Neoplastic Score in Routine Clinical Practice for Patients With Spinal Metastases», *The Oncologist*, vol. 21, n. 1, pagg. 95–101, gen. 2016, doi: 10.1634/theoncologist.2015-0266.

[7] M. C. Costa, P. Eltes, A. Lazary, P. P. Varga, M. Viceconti, e E. Dall'Ara, «Biomechanical assessment of vertebrae with lytic metastases with subject-specific finite element models», *Journal of the Mechanical Behavior of Biomedical Materials*, vol. 98, pagg. 268–290, ott. 2019, doi: 10.1016/j.jmbbm.2019.06.027.

[8] M. L. Ruspi, M. Palanca, C. Faldini, e L. Cristofolini, «Full-field in vitro investigation of hard and soft tissue strain in the spine by means of Digital Image Correlation», pag. 8.

[9] N. Brandolini, L. Cristofolini, e M. Viceconti, «EXPERIMENTAL METHODS FOR THE BIOMECHANICAL INVESTIGATION OF THE HUMAN SPINE: A REVIEW», *J. Mech. Med. Biol.*, vol. 14, n. 01, pag. 1430002, feb. 2014, doi: 10.1142/S0219519414300026.

[10] M. Palanca, M. Marco, M. L. Ruspi, e L. Cristofolini, «Full-field strain distribution in multi-vertebra spine segments: An in vitro application of digital image correlation», *Medical Engineering & Physics*, vol. 52, pagg. 76–83, feb. 2018, doi: 10.1016/j.medengphy.2017.11.003.

[11] M. Palanca, G. De Donno, e E. Dall'Ara, «A novel approach to evaluate the effects of artificial bone focal lesion on the three-dimensional strain distributions within the vertebral body», *PLoS ONE*, vol. 16, n. 6, pag. e0251873, giu. 2021, doi: 10.1371/journal.pone.0251873.

[12] M. R. Hardisty, M. K. Akens, S.-P. Hojjat, A. Yee, e C. M. Whyne, «Quantification of the effect of osteolytic metastases on bone strain within whole vertebrae using image registration», *J Orthop Res*, vol. 30, n. 7, pagg. 1032–1039, lug. 2012, doi: 10.1002/jor.22045.

[13] Cavazzoni Giulia, «In vitro characterization of the three-dimensional strain pattern in human vertebrae affected by metastases».

[14] B. K. Bay, T. S. Smith, D. P. Fyhrie, e M. Saad, «Digital volume correlation: Three-dimensional strain mapping using X-ray tomography», *Experimental Mechanics*, vol. 39, n. 3, pagg. 217–226, set. 1999, doi: 10.1007/BF02323555.
[15] M. Palanca, G. Tozzi, L. Cristofolini, M. Viceconti, e E. Dall'Ara, «Three-Dimensional Local Measurements of Bone Strain and Displacement: Comparison of Three Digital Volume Correlation Approaches», *Journal of Biomechanical Engineering*, vol. 137, n. 7, pag. 071006, lug. 2015, doi: 10.1115/1.4030174.
[16] L. Liu e E. F. Morgan, «Accuracy and precision of digital volume correlation in quantifying displacements and strains in trabecular bone», *Journal of Biomechanics*, vol. 40, n. 15, pagg. 3516–3520, gen. 2007, doi: 10.1016/j.jbiomech.2007.04.019.
[17] B. C. Roberts, E. Perilli, e K. J. Reynolds, «Application of the digital volume correlation technique for the measurement of displacement and strain fields in bone: A literature review», *Journal of Biomechanics*, vol. 47, n. 5, pagg. 923–934, mar. 2014, doi: 10.1016/j.jbiomech.2014.01.001.
[18] M. R. Hardisty e C. M. Whyne, «Whole Bone Strain Quantification by Image Registration: A Validation Study», *Journal of Biomechanical Engineering*, vol. 131, n. 6, pag. 064502, giu. 2009, doi: 10.1115/1.3127249.
[19] G. Tozzi, V. Danesi, M. Palanca, e L. Cristofolini, «Elastic Full-Field Strain Analysis and Microdamage Progression in the Vertebral Body from Digital Volume Correlation: Strain Analysis in the Vertebral Body from Digital Volume Correlation», *Strain*, vol. 52, n. 5, pagg. 446–455, ott. 2016, doi: 10.1111/str.12202.
[20] M. Palanca *et al.*, «Digital volume correlation can be used to estimate local strains in natural and augmented vertebrae: An organ-level study», *Journal of Biomechanics*, vol. 49, n. 16, pagg. 3882–3890, dic. 2016, doi: 10.1016/j.jbiomech.2016.10.018.
[21] R. Müller e P. Rüegsegger, «Micro-tomographic imaging for the nondestructive evaluation of trabecular bone architecture», *Stud Health Technol Inform*, vol. 40, pagg. 61–79, 1997.
[22] T. Hildebrand e P. Rüegsegger, «A new method for the model-independent assessment of thickness in three-dimensional images», *Journal of Microscopy*, vol. 185, n. 1, pagg. 67–75, gen. 1997, doi: 10.1046/j.1365-2818.1997.1340694.x.
[23] R. R. Recker, «Low Bone Mass May Not Be the Only Cause of Skeletal Fragility in Osteoporosis», *Experimental Biology and Medicine*, vol. 191, n. 3, pagg. 272–274, lug. 1989, doi: 10.3181/00379727-191-42919.
[24] M. Kleerekoper, A. R. Villanueva, J. Stanciu, D. S. Rao, e A. M. Parfitt, «The role of three-dimensional trabecular microstructure in the pathogenesis of vertebral compression fractures», *Calcif Tissue Int*, vol. 37, n. 6, pagg. 594–597, nov. 1985, doi: 10.1007/BF02554913.
[25] L. K. Wojnar, A. Gądek-Moszczak, e J. Pietraszek, «ON THE ROLE OF HISTOMORPHOMETRIC (STEREOLOGICAL) MICROSTRUCTURE PARAMETERS IN THE PREDICTION OF VERTEBRAE COMPRESSION STRENGTH», *Image Anal Stereol*, vol. 38, n. 1, pag. 63, apr. 2019, doi: 10.5566/ias.2028.
[26] D. Chappard *et al.*, «Altered trabecular architecture induced by Corticosteroids: A Bone Histomorphometric Study», *J Bone Miner Res*, vol. 11, n. 5, pagg. 676–685, dic. 2009, doi: 10.1002/jbmr.5650110516.
[27] P. I. Croucher, N. J. Garrahan, e J. E. Compston, «Assessment of cancellous bone structure: Comparison of strut analysis, trabecular bone pattern factor, and marrow

space star volume», *J Bone Miner Res*, vol. 11, n. 7, pagg. 955–961, dic. 2009, doi: 10.1002/jbmr.5650110712.
[28] L. Wise-Milestone, M. K. Akens, T. J. Rosol, S.-P. Hojjat, M. D. Grynpas, e C. M. Whyne, «Evaluating the effects of mixed osteolytic/osteoblastic metastasis on vertebral bone quality in a new rat model», *J. Orthop. Res.*, vol. 30, n. 5, pagg. 817–823, mag. 2012, doi: 10.1002/jor.21577.
[29] A. Nazarian, D. von Stechow, D. Zurakowski, R. Müller, e B. D. Snyder, «Bone Volume Fraction Explains the Variation in Strength and Stiffness of Cancellous Bone Affected by Metastatic Cancer and Osteoporosis», *Calcif Tissue Int*, vol. 83, n. 6, pagg. 368–379, dic. 2008, doi: 10.1007/s00223-008-9174-x.
[30] T. Sone, T. Tamada, Y. Jo, H. Miyoshi, e M. Fukunaga, «Analysis of three-dimensional microarchitecture and degree of mineralization in bone metastases from prostate cancer using synchrotron microcomputed tomography», *Bone*, vol. 35, n. 2, pagg. 432–438, ago. 2004, doi: 10.1016/j.bone.2004.05.011.
[31] E. Nägele *et al.*, «Technical Considerations for Microstructural Analysis of Human Trabecular Bone from Specimens Excised from Various Skeletal Sites», *Calcif Tissue Int*, vol. 75, n. 1, pagg. 15–22, lug. 2004, doi: 10.1007/s00223-004-0151-8.
[32] A. M. Briggs *et al.*, «Novel Assessment of Subregional Bone Mineral Density Using DXA and pQCT and Subregional Microarchitecture Using Micro-CT in Whole Human Vertebrae: Applications, Methods, and Correspondence Between Technologies», *Journal of Clinical Densitometry*, vol. 13, n. 2, pagg. 161–174, apr. 2010, doi: 10.1016/j.jocd.2010.01.120.
[33] *Italian Ethical Approval*.
[34] *Ethics Application*.

APPENDIX A

For each specimens, microstructural parameters are reported.

VERTEBRAE AFFECTED BY LYTIC METASTASES

Specimen	**Percent bone volume**	**Trabecular thickness**	**Trabecular separation**	**Trabecular number**
	BV/TV [%]	Tb.Th [μm]	Tb.Sp [μm]	Tb.N [1/mm]
772_T6_L0	0.95	107±38	1505±477	0.09
772_T6_L100	9.02	156±65	852±265	0.58
772_T6_L200	10.47	167±70	824±255	0.63
772_T6_L300	10.99	168±72	787±245	0.65
772_T6_L400	9.93	141±65	744±236	0.70
772_L4_L0	1.03	131±67	2030±897	0.08
772_L4_L100	8.73	19±74	847±304	0.55
772_L4_L200	9.11	151±88	825±292	0.61
772_L4_L300	11.10	163±83	793±267	0.68
772_L4_L400	11.92	156±62	716±235	0.76
772_L4_L500	11.75	128±72	586±303	0.92
772_T11_L0	1.07	131±63	2062±907	0.12
772_T11_L100	7.93	150±68	777±304	0.80
772_T11_L200	7.67	157±73	884±359	0.74
772_T11_L300	7.12	155±71	867±305	0.702
772_T11_L400	5.15	135±63	940±362	0.58
772_T11_L500	5.34	130±64	850±350	0.63
782_T5_L0	1.02	132±62	1665±607	0.08
782_T5_L100	12.20	168±69	778±275	0.73
782_T5_L200	13.79	174±71	896±412	0.79
782_T5_L300	12.14	166±70	868±335	0.73
782_T5_L400	15.39	185±83	790±288	0.83
782_T5_L500	25.67	239±114	579±249	1.70
785_T6_L0	1.03	141±62	2674±1331	0.07
785_T6_L100	18.93	210±99	625±322	0.90
785_T6_L200	17.46	211±96	768±343	0.83
785_T6_L300	12.73	172±79	872±346	0.74
785_T6_L400	16.55	172±70	670±294	0.96

VERTEBRAE AFFECTED BY BLASTIC METASTASES

Specimen	Percent bone volume	Trabecular thickness	Trabecular separation	Trabecular number
	BV/TV [%]	Tb.Th [μm]	Tb.Sp [μm]	Tb.N[1/mm]
777_L2_B-100	75.12	276±108	149±67	2.72
777_L2_B0	71.37	319±145	206±117	2.24
777_L2_B100	26.62	182±94	453±271	1.46
777_L2_B200	21.22	169±85	526±280	1.26
777_L2_B300	27.46	169±85	361±195	1.63
777_L2_B400	34.11	184±106	296±149	1.85
781_T7_B0	45.67	1781±92	319±209	2.12
781_T7_B100	13.44	524±75	957±419	0.76
781_T7_B200	10.82	422±109	958±404	0.61

VERTEBRAE AFFECTED BY MIXED METASTASES

Specimen	Percent bone volume	Trabecular thickness	Trabecular separation	Trabecular number
	BV/TV [%]	Tb.Th [μm]	Tb.Sp [μm]	Tb.N [1/mm]
771_T12_B-100	17.99	202±99	554±264	0.89
771_T12_B0	21.93	244±126	686±373	0.90
771_T12_B100	13.24	187±81	709±357	0.70
771_T12_B200	12.83	189±81	729±384	0.68
771_T12_B300	13.18	200±93	763±368	0.66
771_T12_B400	11.64	181±76	803±378	0.64
771_T12_B500	12.42	162±65	706±303	0.76
771_T12_B600	15.59	158±63	542±234	0.99
771_T12_L0	1.74	140±47	2427±1331	0.12
771_T12_L100	7.41	165±66	1107±471	0.45
771_T12_L200	6.75	160±59	1134±524	0.42
771_T12_L300	8.60	171±65	955±397	0.50
771_T12_L400	8.93	181±76	952±408	0.49
771_T12_L500	10.49	173±66	885±361	0.61
771_T12_L600	11.15	168±64	885±434	0.66
771_T12_L700	12.42	163±62	776±346	0.76
776_L4_B-100	68.50	232±88	268±228	2.95
776_L4_B0	73.59	328±155	271±203	2.24
776_L4_B100	11.36	173±101	809±390	0.66
776_L4_B200	13.70	229±168	844±358	0.60
776_L4_B300	21.21	362±202	866±474	0.59
776_L4_L0	7.60	136±64	499±239	0.56
776_L4_L100	11.19	169±115	642±292	0.66
776_L4_L200	9.95	173±95	755±349	0.57
776_L4_L300	11.05	188±126	834±424	0.59

776_L4_L400	9.95	173±95	755±349	0.57
776_L4_L500	14.57	210±156	724±352	0.69
776_L4_L600	17.83	253±157	675±349	0.70
780_T6_B0	54.61	328±140	550±326	1.66
780_T6_B100	23.65	257±113	686±256	0.92
780_T6_B200	19.74	233±114	702±265	0.85
780_T6_B300	22.68	255±130	709±310	0.89
780_T6_B400	31.79	307±139	583±271	1.04
780_T6_B500	19.25	176±73	537±285	1.09
780_T6_B600	18.08	118±42	157±53	1.53
780_T6_L0	4.31	230±53	1268±538	0.19
780_T6_L100	31.58	343±330	616±330	0.92
780_T6_L200	26.61	277±290	567±290	0.96
780_T6_L300	25.78	260±255	544±255	0.99
780_T6_L400	23.71	214±272	560±272	1.10
780_T6_L500	25.71	213±252	567±252	1.20
781_T12_B-100	93.27	386±134	92±31	2.41
781_T12_B0	65.41	257±114	232±165	2.54
781_T12_B100	8.79	160±74	978±416	0.55
781_T12_B200	6.81	148±62	1032±400	0.46
781_T12_B300	7.73	156±64	1091±558	0.49
781_T12_B400	10.20	170±72	998±464	0.60
781_T12_B500	14.58	187±78	824±329	0.78
781_T12_B600	17.21	190±80	643±278	0.90
781_T12_L0	7.78	121±	998±	0.64
781_T12_L100	10.91	193±	748±	0.56
781_T12_L200	8.22	170±	870±	0.48
781_T12_L300	8.22	170±	870±	0.48
781_T12_L400	8.22	170±	870±	0.48
781_T12_L500	11.86	169±	902±	0.70
781_T12_L600	11.86	169±	902±	0.70
781_T12_L700	6.94	149	945±	0.46

APPENDIX B

For each specimens, minimum principal strains are reported.

VERTEBRAE AFFECTED BY LYTIC METASTASES

Specimen	ε3 (με)
772_T6_L0	-22671±17980
772_T6_L100	-14944±16483
772_T6_L200	-8307±11309
772_T6_L300	-1932±1249
772_T6_L400	-1418±610
772_L4_L0	-9111±5105
772_L4_L100	-10193±6512
772_L4_L200	-9949±9026
772_L4_L300	-9916±10320
772_L4_L400	-9801±10339
772_L4_L500	-8537±8969
772_T11_L0	-6499±10574
772_T11_L100	-6802±15413
772_T11_L200	-8003±15599
772_T11_L300	-11412±13791
772_T11_L400	-12777±2892
772_T11_L500	-13517±1993
782_T5_L0	-21310±1587
782_T5_L100	-196251757
782_T5_L200	-17606±1657
782_T5_L300	-12085±1967
782_T5_L400	-3719±1973
782_T5_L500	-2560±4838
785_T6_L0	-4407±5474
785_T6_L100	-4067±7067
785_T6_L200	-3978±15244
785_T6_L300	-3716±16721
785_T6_L400	-3788±17920

VERTEBRAE AFFECTED BY BLASTIC METASTASES

Specimen	ε3 (με)
777_L2_B-100	-3531±2374
777_L2_B0	-7270±3943
777_L2_B100	-6685±3970

777_L2_B200	-5471±3480
777_L2_B300	-6801±3386
777_L2_B400	-7759±4074
781_T7_B0	-1545±1189
781_T7_B1	-1498±1182
781_T7_B2	-1943±1413

VERTEBRAE AFFECTED BY MIXED METASTASES

Specimen	**ε3 (με)**
771_T12_B-100	-26615±14121
771_T12_B0	-20882±14921
771_T12_B100	-16788±14534
771_T12_B200	-15746±15302
771_T12_B300	-11665±13585
771_T12_B400	-5372±5799
771_T12_B500	-2767±2258
771_T12_B600	-1320±978
771_T12_L0	-20208±15212
771_T12_L100	-16622±14602
771_T12_L200	-13350±11554
771_T12_L300	-13298±11629
771_T12_L400	-10966±11799
771_T12_L500	-8316±10302
771_T12_L600	-6696±11077
771_T12_L700	-6152±11209
776_L4_B-100	-3775±2674
776_L4_B0	-4272±2942
776_L4_B100	-4497±3194
776_L4_B200	-5091±5033
776_L4_B300	-6957±8704
776_L4_L0	-3524±2378
776_L4_L100	-4285±3041
776_L4_L200	-3822±2863
776_L4_L300	-3824±2848
776_L4_L400	-3822±2863
776_L4_L500	-4748±4981
776_L4_L600	-5626±5240
780_T6_B0	-2315±1299
780_T6_B100	-2554±1421
780_T6_B200	-2315±1299
780_T6_B300	-2911±1372
780_T6_B400	-2970±1628
780_T6_B500	-3001±1931

780_T6_B600	-2920±1284
780_T6_L0	-3613±1173
780_T6_L100	-3422±1299
780_T6_L200	-3246±1225
780_T6_L300	-2887±1196
780_T6_L400	-2682±1169
780_T6_L500	-2448±1203
781_T12_B-100	-2467±825
781_T12_B0	-2570±1179
781_T12_B100	-2814±1564
781_T12_B200	-3206±2253
781_T12_B300	-3248±2264
781_T12_B400	-3484±2869
781_T12_B500	-2877±2560
781_T12_B600	-3649±3018
781_T12_L0	-2348±906
781_T12_L100	-2630±1127
781_T12_L200	-2902±2020
781_T12_L300	-3212±2517
781_T12_L400	-3940±3613
781_T12_L500	-4341±3584
781_T12_L600	-4554±3789
781_T12_L700	-3940±3613